# Thermal and charge conductivities of superconducting skutterudite compounds, $PrRu_4Sb_{12}$ and $PrOs_4Sb_{12}$

by

Somayyeh Rahimi

A thesis
presented to the University of Waterloo
in fulfilment of the
thesis requirement for the degree of
Master of Science
in
Physics

Waterloo, Ontario, Canada, 2007

AUTHOR'S DECLARATION FOR ELECTRONIC SUBMISSION OF A THESIS

I hereby declare that I am the sole author of this thesis. This is a true copy of the thesis, including any required final revisions, as accepted by my examiners.

I understand that my thesis may be made electronically available to the public.

**Abstract**

The measurement of thermal conductivity is a powerful probe that can be used for identifying the nature of heat and charge carriers and structure of the gap in the superconducting compounds. At low temperature when the effect of phonons in transporting heat becomes smaller, one can obtain information about the quasiparticle distribution and the superconducting gap structure.

In order to do a sensitive thermal conductivity measurement, we designed and built a thermal conductivity mount. The charge conductivity was measured through the same leads that we used for making the thermal conductivity measurements. To test the mount, we measured the heat and charge conductivity of a silver wire and determined the accuracy with which we could satisfy the Wiedemann–Franz law within 5 %.

We will report the measurements of thermal and electrical conductivities of two filled skutterudite superconducting compounds, $PrRu_4Sb_{12}$ and $PrOs_4Sb_{12}$ at 1.1–35 K temperature range. The differences and similarities between the transport properties of these compounds in the superconducting and normal states along with the results of investigation of the Wiedemann–Franz law will be discussed in the following chapters.

**Acknowledgements**

First and foremost, I would like to thank my advisor Professor Robert W. Hill for his guidance and support during my masters program and providing me with his invaluable feedbacks on this thesis. I admire his patience and enthusiasm in explaining basic ideas and novel concepts of low temperature physics to his students. His vast and priceless knowledge and insight in physics made me realize that so many exciting events happen at low temperature physics.

My special thanks to Professor Jan Kycia. I had the opportunity to discuss our work with him and use his great ideas to improve my experimental methodes and have a better understanding of physical phenomena at low temperatures. I also appreciate his support and helpful feedbacks on my thesis.

I thank Professor Michel J.P. Gingras for his useful suggestions on my committee meetings and giving me the motivation to learn more about the theory which is behind, apparently different but indeed similar systems. I also wish to thank Professor Rob B. Mann for his support for writing my thesis.

Technicians in the science machining shop helped me so much and I am really grateful to all of them, especially Andy Coglough for his help and patience with teaching machining to me. I would also like to thank Nat Persaud for his help with providing endless dewars of helium to our lab.

I would like to thank my dear friend Parisa Bohlouli for her kindness and help through many challenging situations. I admire her logical way of finding an opportunity to learn, in every challenge. I am extremely lucky to have met a remarkable group of friends over the last two and half years, Michael Davenport, Josh Mutus, Joel Vroom, Hamid Reza Molavian, Chas Mugford, Jeffrey Quilliam, Zahra Fakhraei, Shuchao Meng and Lauren Lettress. Their contributions are many and I hope that the friendship bonds continue to strengthen in the future.

My love and affection to my family for their life long support. My especial thanks to my parents who inspired me with the love of science.

*This thesis is dedicated to my parents*

# Contents

# List of Figures

# Chapter 1

# Introduction

The word "Skutterudite" is derived from a town in Norway where minerals with this structure such as $CoAs_3$ were first discovered. Compounds with filled skutterudite structure were discovered by Jeitschko and Braun in 1977 and have the general formula $RM_4X_{12}$. The primitive cell of these compounds has a cubic structure with 34 atoms in the unit cell. This structure consists of a square planar ring of four type "X" atoms with the rings oriented along (100), (010) or (001) directions. The Type "M" atoms form a simple cubic sublattice and the "R" atoms are positioned in the two remaining holes in the unit cell. This structure reduces the thermal conductivity of skutterudite compounds and it gives rise to an increase in thermoelectric power which is defined as $Z = S^2/\kappa\rho$ where S is the thermopower and $\rho$ is the electrical resistivity and $\kappa$ is the thermal conductivity [1].

We worked on two Pr–based skutterudite compounds $PrRu_4Sb_{12}$ and $PrOs_4Sb_{12}$ which have an unusual low temperature properties. By measuring the charge and thermal conductivities of these compounds one can provide a lot of information on the structure of superconducting gap and the type of carriers of heat.

In order to measure the transport properties we designed and built a thermal

conductivity mount which could be used for measuring both electrical and thermal conductivities. In order to do accurate measurements we identified and tried to eliminate possible sources of noise that could affect the experiments. In order to test the veracity of our thermal conductivity data, we used Wiedemann–Franz law which defines a relation between heat and charge conductivities.

Our experiments show that the electrical resistivity of both of these compounds decrease with reducing the temperature which is the typical behavior of the electrical resistivity of metallic compounds. The features in electrical resistivity of both of them can be explained based on electric field of $Pr^{+3}$ ions on electrons of f shells.

The thermal conductivity measurements of $PrRu_4Sb_{12}$ shows that at very low temperatures electrons are the main carriers of heat and impurities play the role of the dominant scattering mechanism. The coupling in the superconducting state of $PrRu_4Sb_{12}$ is most probably weak coupling mediated by phonons.

The analysis of thermal conductivity of $PrOs_4Sb_{12}$ however is more complex from the point of view that some of the features observed in the heat transport depend drastically on the purity level of samples. Although the total picture can be explained based on a combination of electron and phonon effects through different ways, a complete model has not yet been proposed.

# Chapter 2

# Review of theory

## 2.1 Thermal conductivity

In an isotropic solid, thermal conductivity is defined as the coefficient of proportionality between the heat flow vector $\mathbf{j}^q$ and the temperature gradient $\overrightarrow{\nabla} T$ across a solid [2]

$$\mathbf{j}^q = -\kappa \overrightarrow{\nabla} T, \tag{2.1}$$

$\mathbf{j}^q$ is the thermal current density which is a vector parallel to the direction of heat flow whose magnitude gives the thermal energy per unit time crossing a unit area perpendicular to the flow. The negative sign is because the heat flow is from the hotter points towards the colder points.

There are at least two distinct mechanisms for transporting heat in metals, through electrons and phonons. The thermal conductivity due to each mechanism may be calculated separately and the sum of them will give the total conductivity of a metallic system.

$$\kappa = \kappa_e + \kappa_g. \tag{2.2}$$

where both $\kappa_e$ and $\kappa_g$ will be limited by some scattering mechanisms. In the following sections we will discuss the mathematical forms of electronic and lattice thermal conductivities and the scattering mechanisms which affect them.

### 2.1.1 Electronic thermal conductivity and Wiedemann-Franz law

The electron gas in a solid is a quantum gas and the electronic states can be indexed by their band number n and their momentum vector $\mathbf{k}$. The distribution of electrons can be described by the $f(\mathbf{r}, \mathbf{k}, t)$ function which is the same as Dirac-Fermi function in the equilibrium state,

$$f^0(\epsilon_n(\mathbf{k}))\frac{d\mathbf{k}}{4\pi^3} = \frac{d\mathbf{k}/4\pi^3}{e^{(\epsilon_n(\mathbf{k})-\mu)/k_BT}+1}. \tag{2.3}$$

The distribution function can be affected by temperature gradients, external fields and scattering mechanisms. In the presence of the weak external fields, one can neglect interband transitions in 2.3 and let the index n be implicit. In a steady state situation all these effects are balanced against each other. The Boltzmann equation is usually used to describe the steady state distribution,

$$\frac{\partial f}{\partial t} + \frac{\mathbf{F}}{\hbar}\overrightarrow{\nabla}_{\mathbf{k}} f + \mathbf{v_k}.\overrightarrow{\nabla}_{\mathbf{r}} f = (\frac{\partial f}{\partial t})_{collision}, \tag{2.4}$$

where $\mathbf{v_k} = \frac{1}{\hbar}\overrightarrow{\nabla}_{\mathbf{k}}\varepsilon_{\mathbf{k}}$ and $\mathbf{F}$ are the velocity of carriers and external forces respectively. The Boltzmann equation basically expresses that any change in electronic distribution function, $\frac{\partial f}{\partial t}$ could be due to external fields, $-\frac{\mathbf{F}}{\hbar}\overrightarrow{\nabla}_{\mathbf{k}} f$ or diffusion, $-\mathbf{v_k}.\overrightarrow{\nabla}_{\mathbf{r}} f$ or scattering of heat carriers by other particles in the system, $(\frac{\partial f}{\partial t})_{collision}$. The Boltzmann equation is valid provided that the duration of a collision is much smaller than the time between two collisions, ($\tau_c << \tau$). The form of the collision integral $(\frac{\partial f}{\partial t})_{collision}$, depends on the scattering mechanism, however using relaxation

time approximation [2], one can estimate it as

$$(\frac{\partial f}{\partial t})_{collision} = -\frac{f_{\mathbf{k}} - f^0}{\tau_{\mathbf{k}}}, \tag{2.5}$$

where $\tau_{\mathbf{k}}$ is the collision time. Therefore one can assume that the effect of collisions is the exponential evolution of the f towards $f^0$ with a relaxation time of the order of the collision time $\tau$. In the case of isotropic impurity scattering and spatially uniform temperature gradient and electromagnetic fields, f would not depend on $\mathbf{r}$ and if the Fermi surface is isotropic, $\tau$ depends only on $\mathbf{k}$. The thermal current density under those conditions can be written as

$$\mathbf{j}^q = \int \frac{d\mathbf{k}}{4\pi^3} \varepsilon_{\mathbf{k}} v_{\mathbf{k}} (f_{\mathbf{k}} - f^0), \tag{2.6}$$

where $\varepsilon_{\mathbf{k}}$ is the energy of the state $\mathbf{k}$. Using relaxation time approximation, equation 2.5, and in the absence of electromagnetic forces, Boltzmann equation in the steady state regime ($\frac{\partial f}{\partial t} = 0$) can be written as

$$-\frac{f_{\mathbf{k}} - f^0}{\tau_{\mathbf{k}}} = \mathbf{v}_{\mathbf{k}} . \overrightarrow{\nabla}_{\mathbf{r}} f_{\mathbf{k}} \tag{2.7}$$

which can be rewritten as

$$f_{\mathbf{k}} - f^0 = -\tau_{\mathbf{k}} \mathbf{v}_{\mathbf{k}} . \overrightarrow{\nabla}_{\mathbf{r}} f^0 = -\tau_{\mathbf{k}} \mathbf{v}_{\mathbf{k}} . \overrightarrow{\nabla} T \frac{\partial f^0}{\partial T} = \tau_{\mathbf{k}} \frac{\varepsilon_{\mathbf{k}}}{T} \frac{\partial f^0}{\partial \varepsilon_{\mathbf{k}}} \mathbf{v}_{\mathbf{k}} . \overrightarrow{\nabla} T \tag{2.8}$$

and substituting this value for $f - f^0$ in 2.6 one can obtain

$$\mathbf{j}_q = \frac{1}{T} \int \frac{d\mathbf{k}}{4\pi^3} \varepsilon_{\mathbf{k}}^2 \frac{\partial f_0}{\partial \varepsilon_{\mathbf{k}}} \tau_{\mathbf{k}} v_{\mathbf{k}}^2 \cos(\theta) \overrightarrow{\nabla} T, \tag{2.9}$$

where $\theta$ is the angle with respect to the temperature gradient axis and by replacing the integral over $\mathbf{k}$ with an integration over energy

$$\mathbf{j}_q = v_F^2 \tau \frac{1}{3T} \int \varepsilon^2 \frac{\partial f^0}{\partial \varepsilon} N(\varepsilon) d\varepsilon \overrightarrow{\nabla} T. \tag{2.10}$$

Knowing that the specific heat can be written as

$$c_v = \frac{d}{dT} \int \varepsilon N(\varepsilon) f^0(\varepsilon) d\varepsilon = -\frac{1}{T} \int \varepsilon^2 N(\varepsilon) \frac{\partial f^0}{\partial \varepsilon} d\varepsilon, \tag{2.11}$$

comparing 2.10 to 2.1 and using 2.11 one can see that

$$\kappa_e = \frac{1}{3} c_v v_F^2 \tau. \tag{2.12}$$

which is called the kinetic formula and relates the electronic heat transport to heat capacity. The electrical current density can be written as [2]

$$\mathbf{j} = -e \int \frac{d\mathbf{k}}{4\pi^3} v_{\mathbf{k}} (f_{\mathbf{k}} - f^0), \tag{2.13}$$

and knowing that the electrical current density is defined as the proportionality coefficient between the electrical current and electrical field, $\mathbf{j} = \sigma \mathbf{E}$ and doing the same kind of derivation one finds

$$\sigma = \frac{ne^2\tau}{m}. \tag{2.14}$$

Assuming the same scattering time for both thermal and electrical relaxation processes and by dividing 2.10 by 2.14 one can obtain

$$\frac{\kappa_e}{\sigma T} = \frac{\pi^2 k_B^2}{3e^2} = L_0. \tag{2.15}$$

which is called the Wiedemann-Franz (WF) law and the ratio $L_0 = \frac{\pi^2 k_B^2}{3e^2}$ is called the Sommerfeld value of Lorenz number and equals to $2.44 \times 10^{-8} W\Omega K^2$.

One should notice that we used two assumptions in our calculations in this section, the crystal is isotropic and the scattering is elastic. As long as the crystal is isotropic, equation 1.1 is true and WF law is valid only when scattering mechanisms have the same effect on both charge and heat transport and $\tau$ stays the same for both of them which is only true in the case of elastic scattering.

### 2.1.2 Thermal conductivity of phonons

By using the Boltzmann equation for phonons along with the relaxation time approximation and making the Debye approximation which is letting phonon dispersion relation be $\omega = ck$ for all three acoustic branches and assuming a cut–off

frequency for phonon's spectrum, one can obtain

$$\kappa_g = \frac{k_B}{2\pi^2 v_g}(\frac{k_B}{\hbar})^3 T^3 \int_0^{\Theta/T} \tau(x) \frac{x^4 e^x dx}{(e^x - 1)^2}, \tag{2.16}$$

where $\Theta$ is the Debye temperature and $v_g$ is the average phonon velocity and $x = \frac{\hbar\omega}{k_B T}$. The average phonon velocity is given by $v_l \frac{(2s^2+1)}{2s^3+1}$, where s is the ratio of longitudinal to transverse phonon velocity, $\frac{v_l}{v_t}$ [3]. Using Debye theory one can write phonon specific heat as :

$$C_g(x)dx = \frac{3k_B}{2\pi^2 v^3}(\frac{k_B}{\hbar})^3 T^3 \frac{x^4 e^x dx}{(e^x - 1)^2}, \tag{2.17}$$

Knowing that $\tau(x) = \frac{l(x)}{v(x)}$, the lattice thermal conductivity can be written as :

$$\kappa_g = \frac{1}{3} v \int l(x) C_g(x) dx. \tag{2.18}$$

the kinetic equation again.

## 2.2 Scattering of electrons

The mean free path of electrons can be affected by the interaction of electrons with static defects, phonons and other electrons. Assuming that one scattering process is not influenced by the others which are occurring at the same time, one can separately calculate the thermal resistivity due to each scattering mechanism and then add them up to get the total thermal resistivity. This is called Matthiessen's rule. In the following section we will introduce some of the scattering mechanisms and try to find the temperature dependence of them.

### Thermal resistivity due to static defects scattering

The static defects in a metallic compound that includes impurity atoms, vacancies and dislocations will introduce a thermal resistivity which is analogous to the

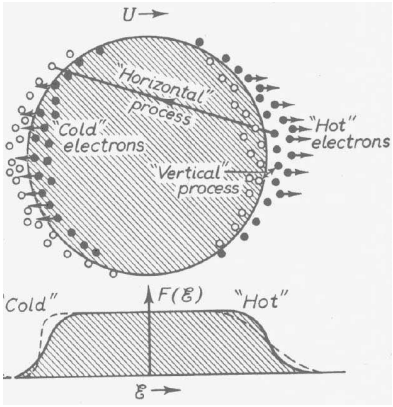


Figure 2.1: Fermi surface and the vertical and horizontal processes

residual electrical resistivity. These defects give rise to a mean free path, l, which is temperature independent. Using kinetic formula, $\kappa = c_v v l/3$ and the fact that electronic specific heat is a linear function of temperature at low temperatures, one can obtain :

$$\kappa_0 = \alpha T. \tag{2.19}$$

where $\alpha$ is a constant. The Wiedemann–Franz law is valid at this temperature range.

### Thermal resistivity due to phonon scattering

The scattering of electrons by phonons can happen through two processes which are called the vertical and the horizontal processes. In a thermal conduction experiment there is no net flux of electrons and so no net flux of charge. The heat current exists because hot electrons travel one way and cold electrons travel the opposite way. So one can describe it as electrons condensing above the Fermi surface and those below the Fermi surface. If a phonon has enough energy it can reverse the direction of electron's velocity, so the electron can move from the right side of the Fermi surface

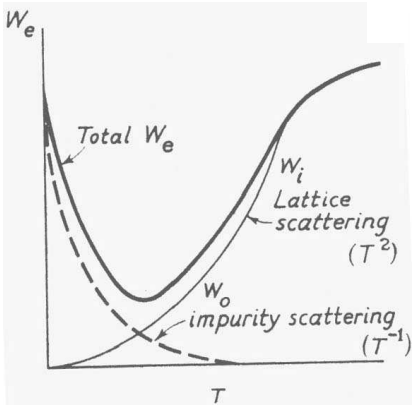


Figure 2.2: Thermal resistivity due to interactions of electrons with impurities and phonons [6]

to the left side. This scattering process is elastic and called the horizontal process and affects both heat and charge conductivity in the same way. In the vertical process which is inelastic, a hot electron loses all its extra energy and falls down below the Fermi level. Such a process has little effect on charge conductivity but affects the thermal conductivity. At low temperatures most of the interactions are inelastic, as the temperature increases, the horizontal process becomes more important since the population of high wave length phonons increases 2.1. At low temperatures when an electron interacts with a phonon, energy of the order of $k_BT$ is either emitted or absorbed by the electron. This energy is enough to transfer the electron from inside of the Fermi surface to the outside and vice versa [5]. The number of phonons present at any temperature is proportional to $T^3$ and so the mean free path of electrons will be proportional to $T^{-3}$. Using the kinetic formula together with the assumption that electronic specific heat, $C_v$, is proportional to T and the velocity is constant [6], one can find

$$\kappa_{e-g} = \beta T^{-2}. \tag{2.20}$$

At higher temperatures the horizontal process affects the heat and charge conductivity in the same way so that one can anticipate the validity of Wiedemann-Franz law. Since at these temperatures, charge conductivity is proportional to $T^{-1}$ using the Wiedemann-Franz law, the electronic heat conductivity will be independent of temperature. Fig.2.2 shows the effect of theses two scattering processes on electronic heat conductivity.

## 2.3 Scattering of phonons

In this section we will review the main sources of scattering of phonons. At very low temperatures boundaries and point defects are the main sources of thermal resistivity against phonons and as the temperature goes up, other phonons and electrons will take their place.

### Thermal resistivity due to lattice boundaries

At low temperatures the phonon mean free path becomes large enough to be comparable to the crystal size. Therefore one can estimate it as the smallest crystal dimensions. Using the kinetic formula $\kappa_g = \frac{1}{3} C_v l v$ and assuming a constant velocity for phonons, the lattice thermal conductivity will be proportional to the phonon's specific heat $\kappa_g \sim T^3$ when the conductance is limited by boundary scattering.

### Thermal resistivity due to conduction electrons

Scattering of phonons by electrons is the dominant scattering mechanism against lattice thermal conductivity in metals. The temperature dependence can be derived by a simple argument. The mean free path of phonons will be proportional to the number of electrons with which they can interact and the only electrons with which

this is possible are those whose energy lies within $k_BT$ of the Fermi energy. The proportion of these electrons to the total number of electrons is $\frac{k_BT}{\varepsilon_F}$, so the mean free path of electrons will change as $T^{-1}$. If one assumes that the velocity of phonons is constant and that $C_v$ is proportional to $T^3$, then from the kinetic theory $\kappa_{g-e} \sim T^2$.

**Thermal resistivity due to phonon–phonon collision**

As the temperature goes up phonon–phonon interactions become more important. In order to find the temperature dependence of phonon thermal conductivity, one can use kinetic formula, $\kappa = \frac{1}{3}Cv\lambda$. At high temperatures, one may suppose that $C \sim 3Nk_B$ and the phonon's velocity is the same as the velocity of sound, s. It is shown in [4] that the mean free path can be expressed as $\lambda \sim \frac{Ds^2}{Nk_BT}\frac{a}{\gamma^2}$, where D and N are the density and number of phonons, a is a length of the order of the lattice constant and $\gamma$ is a constant. Thermal conductivity of lattice can be expressed as :

$$\kappa \sim \frac{Ds^3}{\gamma^2 T}a, \tag{2.21}$$

So lattice conductivity depends on the inverse of the absolute temperature. An inelastic scattering process which is called the Umklapp process or U–process rules the interaction between phonons at intermediate temperature range. In this type of interaction the total momentum of the lattice will not stay reserved, so the heat current associated with the total momentum of the crystal will become dissipated. Thermal conductivity results from Umklapp process can be written as [4]:

$$\kappa \sim T^n \exp(\frac{\beta\theta_D}{T}). \tag{2.22}$$

where n is an exponent that depends on the detail of the model. One can see that as the temperature is reduced, the resistance due to the U–process decreases very rapidly to zero.

## 2.4 Thermal conductivity of conventional superconductors

Superconductors are called conventional when they satisfy the following conditions:

1) The attractive interaction between electrons happens through the exchange of phonons which are called "virtual phonons" and have a short life time.

2) The attraction potential is of the form :

$$V(\mathbf{q}) = V(\mathbf{k} - \mathbf{k}') = \frac{4\pi e^2}{q^2 + k_s^2}, \tag{2.23}$$

where $\frac{1}{k_s}$ is the screening length which is a result of dielectric function of the medium. The potential has no angular dependence and this implies that the gap is a s–wave symmetric gap [8].

One of the first theories to explain the thermal conductivity of conventional superconductors is the two fluid model which was developed by Gorter and Casimir. According to this theory below the transition temperature a certain fraction of electrons, $1-x$, which are called normal electrons occupy the states above the Fermi surface and the rest of electrons, $x$, which are superconducting electrons occupy the states below the Fermi level. The superconducting fluid has two properties :

1) It carries no entropy

2) The electrons in this fluid are not scattered by phonons and impurities

As the specific heat of the superconducting fluid is zero they can not contribute to the heat transport, therefore as the temperature is reduced below $T_c$ fewer electrons can carry the heat and so the thermal conductivity decreases. The relative change in the thermal conductivity due to entering to the superconducting state is larger than the relative change of that in the field induced normal state below $T_c$.

One can have a nice qualitative picture of the heat transport in the superconducting state based on the two fluid model, although this model is not sufficient to explain all the details. One of the puzzles that this model was unable to solve is the difference in the slope of $\frac{\kappa_s}{\kappa_n}$ as a function of normalized temperature when the dominant scattering mechanism against electrons is either phonons or impurities. Based on experimental facts this slope is zero when the dominant scattering mechanism is impurities and is 5 when phonons are the most important scattering mechanism. In order to have a more quantitative picture of what happens below $T_c$ one can use the theory developed by Bardeen, Cooper and Schrieffer and usually refers to as the BCS theory.

The basic idea in the BCS theory is that even a weak attraction can bind pairs of electrons into a bound state. The bound state is a configuration of electrons in which states of electrons of equal but opposite momentum and spin, $(\mathbf{k}\uparrow, -\mathbf{k}\downarrow)$ are both either occupied or unoccupied. The instability of the Fermi sea against the formation of these pairs causes a gap of order of $k_BT_c$ in the excitation spectrum $E(\mathbf{k}) = (\varepsilon(\mathbf{k})^2 + \Delta(\mathbf{k})^2)^{0.5}$ where $\varepsilon(\mathbf{k})$ is the energy of an electron of wave vector $\mathbf{k}$ in the normal state. Cooper pairs have the properties of a superconducting fluid in two fluid model; they carry no entropy and do not scatter phonons. The first statement says that the electronic thermal conductivity decreases upon entering into the superconducting state. Since $\kappa_e \sim nvl_e$ and $n$ changes exponentially with temperature below $T_c$, one can see $\kappa_e \sim exp(-\frac{\Delta}{k_BT})$ at low temperatures. Provided that the mean free path of phonons is limited by electron–phonon scattering, the second condition implies that the thermal conductivity of phonons will increase upon entering the superconducting state, so a competition between decreasing $\kappa_e$ and increasing $\kappa_g$ will determine the overall dependence of thermal conductivity on temperature. In a vast majority of conventional superconductors, thermal conductivity decreases as the material goes superconducting. The theory of heat transport in conventional superconductors has been discussed in [9]. In the following section

we will discuss it briefly.

### 2.4.1 Electronic thermal conductivity in BCS superconductors

When the electron–impurity scattering is the dominant scattering mechanism, the velocity, $v_k$, and scattering time, $\tau_s$, of quasiparticles can be expressed in terms of the same variables of the normal state using the following equation:

$$v_k = |\frac{\varepsilon_k}{E_k}|v_F, \tag{2.24}$$

and

$$\tau_s = |\frac{E_k}{\varepsilon_k}|\tau_N. \tag{2.25}$$

where $E_k$ and $\varepsilon_k$ are the energy of carriers in the superconducting and normal states and $\tau_N$ is the relaxation time in the normal state. Therefore at the Fermi level when $k \to k_F$ and $\varepsilon_k \to 0$ the velocity of quasiparticles will go to zero and the scattering time diverges which means that the impurity ions have very little influence on low energy quasiparticles. One can see that the mean free path of quasiparticles does not change comparing to that of normal electrons. Using 2.24 and 2.25 it is shown in [9] that the electronic thermal conductivity in the superconducting state can be expressed as :

$$\kappa_{e,s} = \frac{2F_1(-y) + 2yln(1+e^{-y}) + y^2/(1+e^y)}{2F_1(0)}, \tag{2.26}$$

where

$$y = \epsilon_0/k_BT, \tag{2.27}$$

and

$$F_n(-y) = \int_0^\infty \frac{z^n dz}{1+e^{x+y}}. \tag{2.28}$$

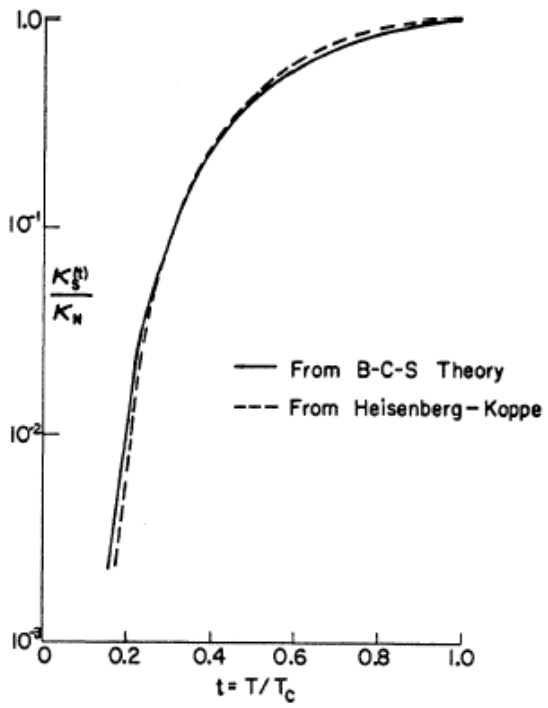


Figure 2.3: Electronic thermal conductivity predicted by Bardeen et. al comparing to the results of Heisenberg–Koppe model which is in agreement with the experiment [9]

A plot of the electronic thermal conductivity, dominated by electron–impurity scattering, predicted by this theory and the prediction of the Heisenberg and Koppe model which is a modification of the two fluid model has been displayed in fig.2.3. The results of Heisenberg–Koppe model is also in agreement with the experimental data [9]. This results is valid for non–magnetic impurities. The magnetic impurities which break the time reversal symmetry can lead to a strong depression of $T_c$ and a modification of the BCS density of states so that it becomes gapless for a finite range of concentration below a critical value which destroys superconductivity entirely [8].

If the dominant scattering mechanism for electrons in the superconducting state is electron–phonon interactions, then the thermal resistivity due to this mechanism can be written as:

$$\kappa_e = \frac{\pi^2 n}{3m} k_B^2 T (\Gamma + v_F/l)^{-1}, \tag{2.29}$$

where $\Gamma \sim T^3$ results from the phonon absorption and emission and $v_F/l$ is independent of temperature. In general, the ratio of electronic thermal conductivity in the superconducting state to that of normal state is a universal function of $\frac{T}{T_c}$ when one scattering mechanism dominates,

$$\frac{\kappa_{e,s}}{\kappa_{e,N}} = \frac{\int_{\Delta(T)}^{\infty} dE E^2 (-\frac{\partial f}{\partial E})}{\int_0^{\infty} d\varepsilon \varepsilon^2} \frac{\partial f}{\partial \varepsilon}. \tag{2.30}$$

### 2.4.2 Thermal conductivity of the lattice

By solving the Boltzmann equation for phonons in the superconducting state one can find the following formula for lattice thermal conductivity:

$$\kappa_{gs} = D(T/\Theta)^2 \int_0^{\infty} \frac{u^3 du}{(e^u - 1)(1 - e^{-u}) g(u)}, \tag{2.31}$$

where D is a constant independent of temperature and

$$g(u) = \frac{1 - e^{-u}}{u} \int dE |\frac{EE'}{\epsilon\epsilon'}| (1 - \frac{\epsilon_0^2}{EE'}) f(E) f(-E'). \tag{2.32}$$

All the energies are measured in units of $k_BT$. One can compare it to the lattice thermal conductivity in the normal state when the dominant scattering mechanism is electron–phonon interactions,

$$\kappa_{g-e} = D((T/\Theta)^2) \int_0^\infty \frac{u^3 du}{(e^u - 1)(1 - e^u)} = 7.2D(T/\Theta)^2. \tag{2.33}$$

In conclusion, we defined the conventional superconductors as the compounds in which electron–phonon interactions give rise to a weak coupling between electrons. This coupling gives rise to an isotropic s–wave energy gap. We saw that lattice conductivity is not affected too much by the transition from the normal state to the superconducting state. However since the superconducting electrons do not carry heat, the phase transition can give rise to a decrease in the electronic heat transport.

## 2.5 Thermal conductivity of unconventional superconductors

The difference between the conventional and unconventional superconductors can be in the gap symmetry and type of interactions which give rise to the formation of Cooper pairs. The symmetry of the order parameter in unconventional superconductors comparing to BCS superconductors is reduced so that there might be gapless excitations even for the pure specimens. Such superconducting states have been observed both in heavy fermions, cuprates and some biomaterial compounds. The nodal structure on the Fermi surface of unconventional superconductors can be a series of line nodes or point nodes. The theory of electronic thermal conductivity in unconventional superconductors with line nodes has been discussed in [10]. For a clean superconductor with an order parameter that vanishes along a line on the Fermi surface, the density of states is a linear function of the excitation energy,

$N(\epsilon) = N_F \frac{\epsilon}{\Delta_0}$ for $\epsilon < \Delta_0$. Because of impurity atoms, the density of states is approximately constant and non zero below an energy level, $\gamma$. For an order parameter with a line of nodes, the bandwidth, $\gamma$, and the density of bound states at zero energy, $N(0)$, are finite for any finite concentration of impurities. The electronic conductivity for an unconventional superconductor with an order parameter that vanishes along a line of nodes when the frequency of the voltage decreases to zero has been shown to have a universal limiting value, $\sigma_0 = \sigma(T = 0) \simeq e^2 N_F v_F^2 \tau_\Delta$ where $\tau_\Delta \simeq \frac{\hbar}{\pi \Delta_0}$ is a universal transport time [11].

The universal limit is most easily realized in the strong scattering limit. There is considerable evidence that some of the heavy fermion superconductors have an order parameter with a line of zeros on the Fermi surface. It has been discussed in [10] that the component of the electronic thermal conductivity tensor corresponding to quasiparticles in the vicinity of line nodes are determined by the same scattering rate as the electrical conductivity and are universal in the limit $T \to 0$. Therefore WF law is obeyed for the ratio of the universal electrical and thermal conductivities in the limit $k_B T \ll \gamma$. The thermal conductivity in this vicinity can be expressed as :

$$\kappa \sim N_F(\gamma/\Delta_0) k_B^2 T v_F^2 (\hbar/\gamma) \sim N_F v_F^2 k_B^2 T (\hbar/\Delta_0). \tag{2.34}$$

The ratio of universal thermal to electrical conductivities gives the Sommerfeld value for Lorenz ratio, $L_0 = 2.44 \times 10^{-8}$. For temperatures above the crossover energy $k_B T \geq \gamma$, the Lorenz ratio $L(T)$ deviates significantly from the Sommerfeld value. For very clean superconductors $L(T)$ is larger than $L_0$ but for higher impurity levels $L(T)$ will be smaller than $L_0$.

For lattice contribution to thermal conductivity at sufficiently low temperatures one can expect the boundaries of the lattice be still the main reason for scattering phonons so $\kappa_g \sim T^3$ can be used in the superconducting regime of unconventional superconductors. It has been discussed in [12] that the lattice conductivity in the

case that quasiparticles dominate the scattering of phonons can be expressed as

$$\begin{aligned}\kappa_g(T) &= A(\frac{T}{T_c})\int_0^\infty dx \frac{x^4 e^x}{(e^x-1)^2} \times [1+\alpha x^4 \frac{T^4}{T_c^4} \\ &+ \beta x^2 \frac{T^4}{T_c^4} + \delta x \frac{T}{T_c} + \gamma x \frac{T}{T_c} g(x,y)]^{-1}.\end{aligned}$$

where $x = \hbar\omega/k_B T$ is the reduced phonon energy and $y = \frac{\Delta(T)}{k_B T}$ is the parameter containing the energy gap.

In conclusion in this chapter the different mechanisms that participate in conducting heat in normal metals and BCS and unconventional superconductors have been investigated. Along with these mechanisms the most important interactions that give rise to scattering the heat carriers at different temperature ranges have been discussed. In the following chapters those results will be used to estimate the contributions of electrons and phonons in heat and charge transport of two skutterudite compounds.

# Chapter 3

# Experimental Details

In this chapter I will introduce the instrumentation which we used for making our thermal conductivity and resistivity measurements. I will briefly review the definition of thermal conductivity, the steady state technique that we used for doing the heat transport measurements and the modification which we did for making more accurate measurements.

## 3.1 $^4He$ Cryostat

The thermal conductivity and resistivity measurements presented in this thesis were performed using a $^4He$ cryostat which was insertable into a liquid helium dewar. In order to go down to temperatures below 4 K we pumped on a small storage of liquid $^4He$.

### 3.1.1 Wiring

Fig.3.1 shows a diagram of a $^4He$ cryostat that is very similar to what that was used in our measurements. The part that goes into the $^4He$ bath, consists of a small

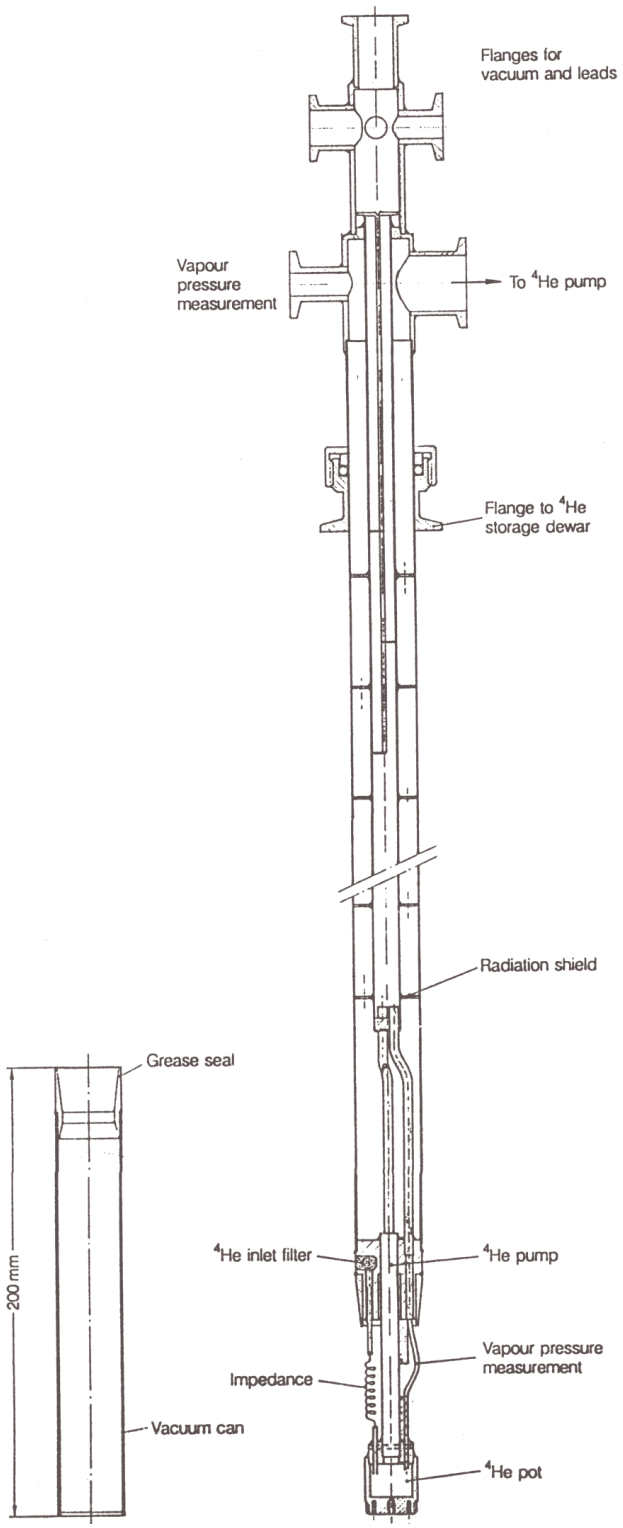


Figure 3.1: Schematic picture of a $^4He$ cryostat from [13]

helium storage volume which is called the 1K pot and is inside the vacuum can in which sample holder, heaters and sensors of the temperature controlling system are located. At the other end of this instrument are the valves used to control the pressure inside the vacuum can and 1K pot. The 1K pot is in direct contact with a brass and a copper block that sample holder is connected to. The wiring that was used for performing measurements was inside teflon tubing located between the sample holder at one end and the temperature controller at the other end of the cryostat. The wires were chosen to give the minimum heat leak through the wiring setup. One could use either copper wires with a relatively high thermal and electrical conductivity, or constantan wires which have a low thermal and electrical conductivity comparing to copper. Using either of them has its own advantages and disadvantages. In the case of copper wires, one could pass relatively greater currents through the wires without worrying too much about the heat generated inside the wiring setup, since the heat generated by this current is proportional to resistance of the wire. However because of their high thermal conductivity, a lot of heat might be conducted across them into the cryostat. In the case of constantan, this reasoning is reversed. As a result of high electrical resistivity, one can not pass a current as high as that of copper through them, although having a low thermal conductivity helps them not to conduct a significant amount of heat into the instrument. We noticed that the optimal case was to use a combination of both constantan and copper wires. A combination of 4 copper wires with diameter 50 $\mu m$ and 8 constantan wires with diameter 120 $\mu m$ and 120 cm long were used. Table 2.1 exhibits the thermal conductivity and conductance of these wires at room temperature and 4 K. Since the temperature along this wiring changes between 4 K at one end and room temperature at the other end, in order to calculate thermal conductivity, one needs to consider the average conductivity of them. According to table 1, the average value of thermal conductance of constantan is 0.18 $W(cmK)^{-1}$ and that of copper is 5.7 $W(cmK)^{-1}$. The maximum heat is transferred through

| | $\kappa(4K)$ | $\kappa(300K)$ | $\kappa(Avg)$ | $Conductance(\mu W/K)$ |
|---|---|---|---|---|
| *Copper* | 3 | 4 | 5.7 | 0.93 |
| *Constantan* | 0.0022 | 0.1307 | 0.18 | 0.17 |

Table 3.1: Thermal conductivity ($W/cmK$) and the average conductance of the wires passing through the cryostat [15]

the wiring when one end of the cryostat is at 4 K and the other end is at room temperature. In this case the heat conducted via the constantan wires would be 51 $\mu W$ and 280 $\mu W$ through copper wires. Therefore the heat conduction of copper wires is about 5.5 times larger than that of constantan wires. Comparing the electrical resistance of the constantan wires to that of copper wires, the ratio of heat generated inside the constantan wires to that generated into copper wires as a result of passing equal electric currents through them will be 4. So at the same time that copper transports a heat 5.5 time bigger comparing to that transported by constantan, the heat generated inside constantan wires as a result of passing current through them would be 4 time larger than that of copper wires.

### 3.1.2 Heater and thermometry system

The temperature was controlled by a model 331 LakeShore temperature controller. A calibrated Cernox resistance temperature sensor and a heater were set up with the temperature controller. The temperature sensor was mounted in a brass block between the 1K pot and the block where the sample holder is mounted. Since the cooling power of 1K pot and the output of the heater might affect the thermal conductivity measurements, the brass plate makes a weak thermal link between the mount and the temperature controlling setup. The controller balances the amount of heater power against the cooling power available at 1K pot to provide

a stable temperature. In order to control the heater output we needed to set three parameters on the temperature controller which we would call P–I–D setting. The complete table of these parameters is listed in a separate report [16]. To improve our thermometry ability, we mounted a calibrated Cernox thermometer close to the sample holder. The issues related to this reference thermometer will be discussed in section 2.6.

### 3.1.3 Vacuum can

A tapered grease seal is used to hold the vacuum can in place. We used a turbo pump to make a vacuum below $10^{-4}$ mbar in the vacuum can. In order to minimize the heat loss through convection the vacuum for making thermal conductivity measurements should be less than $10^{-4}$ mbar. One should notice that at liquid helium temperature the vacuum is much higher because all the non–helium gas molecules are cryopumped to the side of the vacuum can.

### 3.1.4 Cooling procedure

In order to obtain temperatures below 4 K, one needs to pump on a liquid helium bath to remove the more energetic molecules. This is not very efficient, because about 40 % of the liquid $^4He$ has to be evaporated to cool it from 4.2 K to 1.3 K, due to the large magnitude of the specific heat and latent heat in this temperature range. On the other hand, the specific heat of solids is rather small, in comparison to the liquid $^4He$, at this temperature range [13], so to cool them from 4.2 K to 1.3 K, we have to evaporate only a small fraction of liquid $^4He$. It is therefore much more efficient to leave the main part of the liquid at its normal boiling point and just pump on a small fraction of it in a separate container to reach the lower temperatures for the experiment. Fig.3.2 shows a schematic picture of the 1K pot

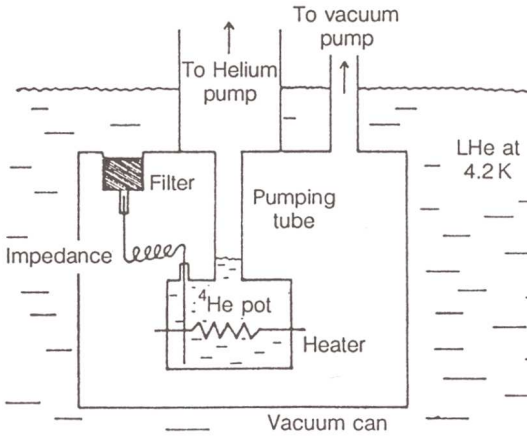


Figure 3.2: Schematic picture of 1K pot and the cooling and heating configuration from [13]

inside the $^4He$ bath. Inside the cryostat tubing is attached to the pot which is connected to a tee at room temperature that is controlled by two valves, one of them is attached to the pump, for pumping on liquid helium inside the pot and the other one is used for flushing the tube with helium right after moving the cryostat into the helium dewar. A rotary pump was used for pumping on the 1K pot. Continuous refill of the pot is provided by a thin capillary attached to the pot and is controlled by a needle valve. In order to make a balance between the cooling power and the heat generated by the heater of the temperature controller, we used a needle valve which adjusts the opening of the pot. Although this refill facility seems very simple in principle, it took a few weeks before getting it to work properly. One of the main problems in running the system was the blocking of the opening of the pot due to air getting trapped and frozen at 77 K, the freezing point of liquid nitrogen. Ice at the opening of the pot would not let the needle valve be adjusted properly. To resolve this problem we would flush the capillary tube connected to 1K pot with helium gas before cooling the system down. To operate continuously below 3.5 K, we need to let the liquid helium into the 1K

pot continuously by adjusting the needle valve. Careful adjustment of the needle valve is required, since having the helium enter the pot too quickly would not let the temperature come down, because the liquid coming into the pot is at 4 K. One could also pump on helium gas in order to stabilize the system at 4 K and above.

## 3.2 Thermal Conductivity Measurements

### 3.2.1 Description

We used a 4–probe method for doing our thermal conductivity measurements. In this method the sample must be connected to a cold bath at one end and a heater at the other end and two thermometers in between for measuring the temperature gradient. To measure thermal conductivity we used the longitudinal steady-state method. For every temperature step, the temperature of the sample is stabilized at some temperature $T_0$, and then by using a heater connected to one end of the sample, we applied a constant heat to one end of the sample. At equilibrium the temperature gradient across the sample is measured by two thermal sensors. Then the thermal conductivity is given by

$$\kappa = \frac{\dot{Q} \times \alpha}{\Delta T}. \tag{3.1}$$

where $\dot{Q}$, $\alpha$ and $\Delta T$ are the heat flow through the sample, the geometric factor and the temperature gradient along the sample respectively. For making an accurate measurement of thermal conductivity, all the heat dissipated by the heater has to go through the sample. Thus, the setup is designed to limit heat losses through the wires connecting to the thermometers and heaters.

### 3.2.2 Thermal conductivity mount

A copper thermal conductivity mount was used for doing the measurements. Copper is a relatively good conductor of heat and has a small heat capacity. Both of these properties help to produce negligible temperature gradient across the frame and between different components of the circuit. The $\kappa$–mount is a 2.5×3.5 cm copper frame that we could screw into a copper block connected to the 1K pot and temperature controlling plate, located inside the vacuum can. Thermometers and heater must be thermally and electrically isolated from the copper block and were suspended on kapton ribbons. The low thermal conductance of kapton ribbons makes a perfect thermal isolation for thermometers and heaters. In order to have an accurate reading for the temperature of each end of samples, there must be good thermal links between the temperature sensors and samples. We used 50 $\mu m$ silver wires to connect the sample to the heaters, sensors and the ground. The conductance of these thermal links was 400 $\mu W K^{-1}$ which was high comparing to the conductance of samples we used. The resistances of temperature sensors and heaters were measured through the coils made from a 25 $\mu m$ insulated constantan wire. the thermal conductivity and conductance values of these wires are given in table 2.2. As mentioned before, constantan has a small thermal conductivity which helps to keep the sensors thermally isolated. Fig.3.3 and 3.4 display a real and schematic picture of $\kappa$–mount we used in our measurements.

#### Thermometers

The temperature sensors that we used for doing our measurements were Cernox CX–1050–BG from LakeShore. They are semiconducting resistors with a surface area of 1.5×1.5 $mm^2$ and are sensitive above 1 K. The Cernox thermometers had a gold substrate that we used for soldering an attachment to it. This attachment consists of a 25 $\mu m$ insolated silver wire wrapped around a 100 $\mu m$ bare silver

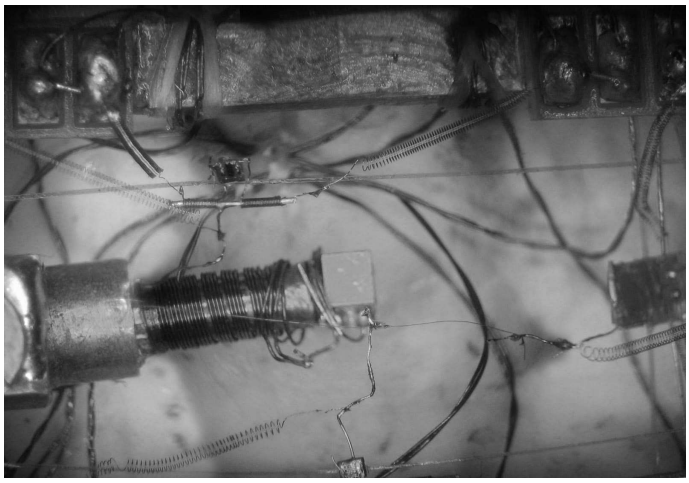

Figure 3.3: Thermal conductivity mount that we used in our experiments, a piece of silver wire as the sample is mounted between the heater and the ground

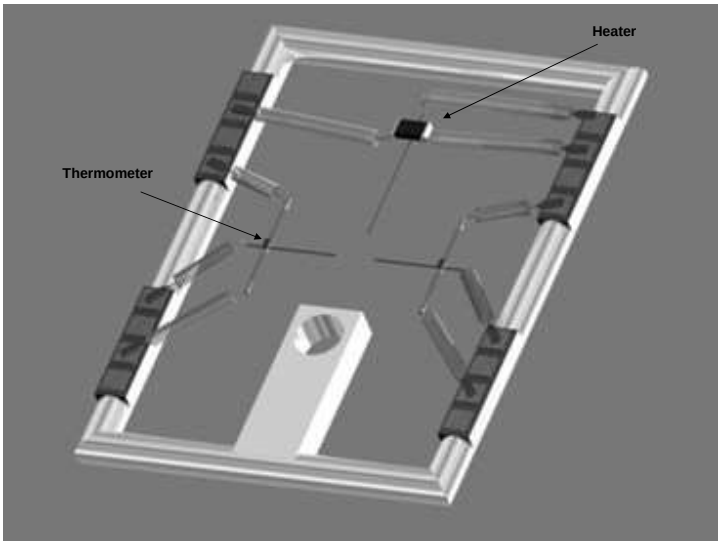


Figure 3.4: Diagram of the thermal conductivity mount, the heater and two thermometers suspended on kapton ribbons along with constantan coils used for making resistivity measurements are shown in the diagram. A schematic picture of the mount and the heat flows are shown in fig.3.7

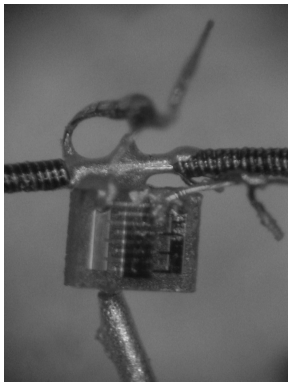

Figure 3.5: Thermometry setup that we used to measure the temperature of the sample

wire that is thermally attached to the sample. Wrapping the insulated wire around the bare silver wires maximizes the thermal contact between the sample and the sensors. Fig.3.5 shows the thermometry setup we used in our measurements. The problem that usually happened here is that the insulation layer of the wrapped silver wire would crack and make a short between the wires. To avoid this problem, we put some GE varnish on the coils to make an extra insulation layer on them. The other ends of coils were soldered to the constantan insulated coils mentioned in the last section. The room temperature resistance of the thermometers was 60 Ω and increased to about 20000 Ω at 4 K.

**Heaters**

The heaters were transducer-glass strain gauges resistors from Vishay Micro-measurements company. They were 5 kΩ resistors and we used two of them in series. Their resistances have a weak temperature dependence, so that by reducing the temperature from room temperature to 4 K their resistance changed by a factor 1 %. In order to have a good thermal contact between them, we glued a piece of copper sheet between them. A DAQ output of the Lock–In Amplifier was used as a voltage

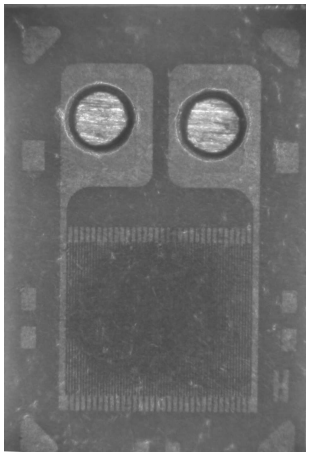

Figure 3.6: The heaters are strain gauges resistors with $2.3 \times 3.9mm$ dimensions

source for the heaters.

### 3.2.3 Sample preparation and mounting

In order to be consistent on the geometric factor used for calculating the thermal conductivity and electrical resistivity of our samples we used the same contact for all the samples, so the error in the Wiedemann-Franz law due to the geometric factor would be zero. A four wire method was used for measuring electrical resistance of the samples. An electric current was passed through the samples from the contacts at both their ends, and the voltage drop was measured between two different points on the samples. The advantage of this method is that it avoids the resistance of contacts in the sample resistance measurement. The current contacts were silver wires of 50 $\mu$m diameter and voltage ones were silver wire of 25 $\mu$m diameter soldered on the sample by indium solder. Soldering the contacts on the skutterudite samples was done by Rob Hill. In order to avoid touching the sample directly by the

soldering iron, silver wires were heated up so that indium solder on them became melted and then we put the hot wires on the sample.

In order to measure the geometric factor of the samples, we took pictures of the samples under a microscope and then by scaling the dimensions of samples against a piece of fine silver wire with 50 $\mu m$ diameter, made an estimation of the dimensions of the samples. It is obvious that the accuracy of measurements is confined to the quality of the pictures and how well we could scale the measurements against the dimensions of the silver wire.

## 3.3 Electrical Resistivity Measurements

For measuring the resistance of the thermometers and the sample, we used an AC resistance bridge, LR–700 from Linear research Inc. The bridge uses a signal with 16 Hertz frequency for measuring the resistance and inductance.

In order to read the resistance of a temperature sensor, one needs to measure the voltage across the sensor due to a current flowing through it. The level of noise in the circuit is inversely proportional to the voltage used for making the measurement and the heat generated into the system is proportional to the square of this voltage, $P = \frac{V^2}{R_{heater}}$. The main challenge in reading the resistance of thermometers cames up at very low temperatures. At low temperatures when the resistance of sensors is large, one needs to use a small current to avoid generating too much heat in the system and at the same time the current should not be too small to give rise to an inaccurate measurements.

The resistance of the samples we used was smaller than sensor's by a factor of $10^7$. So the excitation current needed for samples could be larger than that of sensors. however since the samples were thermally connected to the sensors, one needs to consider the issue of generating unwanted heat very carefully. Further

| | *Silver* | *Constantan* | *Kapton* |
|---|---|---|---|
| $Conductivity(4K)$ | 10 | 0.0022 | 116.622E-6 |
| $Conductance(4k)$ | 78.5 | 0.004 | 2.04E-6 |
| $Conductance(300K)$ | 33.8 | 0.257 | 140.04E-6 |

Table 3.2: Thermal conductivity ($W/cmK$) and conductance ($\mu W/K$) of the thermometry setup at 4 K and room temperature

discussion has been made on unwanted heat, in the section on self heating issue.

## 3.4 Heat Losses channels

Heat losses is a crucial consideration one needs to keep in mind while measuring thermal conductivity. This comes from the question of knowing how much heat is traveling through the sample. There are three potential sources of heat loss: via conduction, radiation or convection. Conduction will happen mostly through the measurement wires, secondly through photons and the least through the remaining gas in the experimental chamber.

### 3.4.1 Losses through conduction

Fig.3.7 is a schematic of the Kappa mount that is showing the possible paths for heat to flow. In the ideal case all of the applied heat generated by the heater flows through the sample and goes to the copper frame at the end of path 1. In the real case it can follow two parallel thermal paths as shown in fig.3.7 The first is through the sample (path 1) and the second is through the measuring wires of the heater (path 2). Two more paths are in the way of heat current as it flows through the sample, the measuring wires of the thermometers (paths 3,4). Since

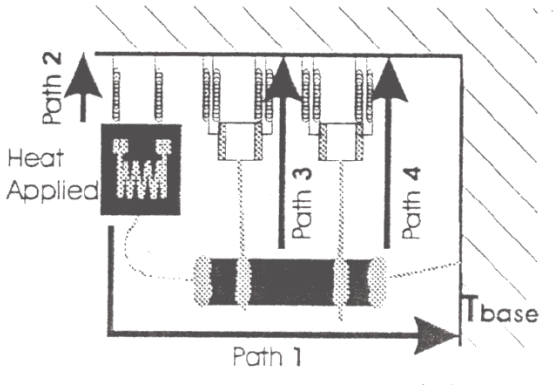


Figure 3.7: The heat stems from the heater will flow paths 1 to 4. Avoiding heat losses is obtained by having most of the heat go through path 1

the thermometers are suspended on Kapton ribbons, they could be a potential way for the heat to go through. The Kapton ribbons have not been labeled in fig.3.7 and will be considered as parts of path 3 and 4 in the following calculations. In order to have most of the heat through the sample, the last three paths must have a much smaller thermal conductivity comparing to that of the sample.

The constantan coils were 10 cm long and had a 25 $\mu m$ diameter and the silver wires used for having the sample connected to the sensors were 0.5 cm long and had a 25 $\mu m$ diameter. The kapton ribbons were type HN of 0.007 $mm^2$ cross section and about 2 cm long and their thermal conductivity can be expressed as $\kappa = 30T^{0.9794}\mu W/cmK$ in 4 K–300 K [14]. The thermal conductance of different components of these four paths has been gathered in Table 2.2. By considering the fact that thermal conductance of the samples we used was of the order of 10 $\mu WK^{-1}$ at 4 K one can see that path 1 has the least thermal resistivity.

### 3.4.2 Losses through radiation

The Stephan–Boltzmann law of radiation states the power dissipated by a black body is proportional to $T^4$. So the radiation problem becomes more important at higher temperatures. For two parallel plane surfaces of emissivities $\epsilon_1$ and $\epsilon_2$ at temperatures $T_1$ and $T_2$, the heat transferred by radiation from a surface area of A per unit time is [15]:

$$\dot{Q} = \sigma A[{T_2}^4 - {T_1}^4] \times \frac{\epsilon_1 \epsilon_2}{\epsilon_1 + \epsilon_2 - \epsilon_1 \epsilon_2}. \tag{3.2}$$

where $\sigma = 5.67 \times 10^{-8} W m^2 K^4$ is the Stephan–Boltzmann constant. Emissivities have a maximum value equal to 1 for a perfect black body. For a thermal conductivity setup each component will radiate a certain amount of heat while no heat current is applied. They will then radiate an additional amount of heat when the heat current is passing through them. Therefore the losses due to radiation mainly come from all parts of the setup (including the sample) which has a higher temperature when a heat current is applied. The main component will be the heater which has the highest temperature, but the sample and thermometers also contribute.

### 3.4.3 Losses through convection

In order to achieve thermal isolation through a vacuum the vacuum should be significantly better than $10^{-3}$ mbar. Below that pressure the thermal conductance of the residual gas in the vacuum will be approximately proportional to its pressure. Since the pressure in the sample chamber is typically much less than $10^{-4}$ mbar, the mean free path of the gas molecule, $\lambda$, is larger than the dimensions of the can;

$$\lambda = \frac{1}{\sqrt{2}\pi d^2 n}. \tag{3.3}$$

where $d$ is the diameter of a molecule and $n$ is the number of molecules per unit volume. In that case the power lost by convection through the residual gas is given

by the following relation [15]:

$$Q_{convection} = \frac{constant}{\sqrt{T}} \times a_0 p(T_2 - T_1).Wm^{-2} \tag{3.4}$$

where p is the pressure of the gas, $T_1$ and $T_2$ are the temperatures of the two points between which heat is exchanged, and $a_0$, the accommodation coefficient which is always smaller than 1. For conduction in air, $constant/\sqrt{T} \approx 0.12$ at 4 K. There would be a small heat exchange between the sample holder at 1.5 K and the wall of the can at 4 K. When the heater is on, the temperature of sample holder increases to 2 K and so $\Delta T = 2K$, the heater surface area is 7.7 $mm^2$ and thus $Q_{convection} = 1.52nW$ from the surface area of the heaters. This is negligible comparing to the heat applied to the sample which is about 200 $\mu W$.

## 3.5 Self heating issues

In order to make an accurate thermal conductivity measurement, we need to know the amount of heat that is flowing via the sample and other components of the circuit. Since the heat capacity of most materials is lower at lower temperatures, a small amount of heat can warm up the setup more at lower temperatures. Therefore the effect of self heating is more noticeable at low temperatures. Self heating issue can comes up in two different ways :

1) Self heating that affects accurate thermometry in either thermal conductivity or electrical resistivity measurements. This occurs when the current used to measure the resistance of the sensor generates a lot of heat in the sensor itself and therefore makes it hotter than it would be if the measuring current were not applied.

2) Self heating of the sample due to excess current when measuring its resistance. This means that the sample gets warm and the thermometers are not necessarily at the same temperature as the sample. This kind of self heating is rarely due to

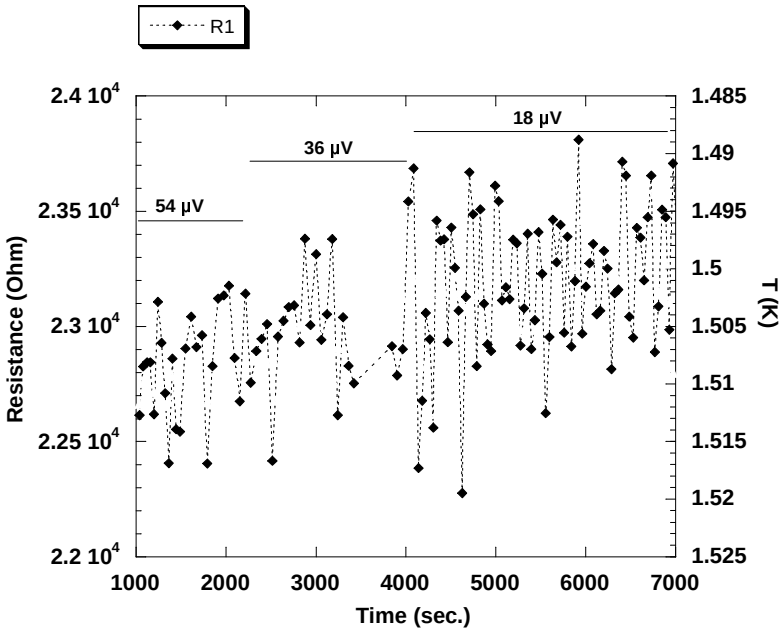


Figure 3.8: The effect of setting three different excitation voltages on the resistance of one of the thermometers

the sample resistance as it is usually very small and is mostly due to the contacts which can have a large resistance relative to the sample or the constantan coils which are attached to the sample. In order to cure these problems one can consider the following solutions :

1) In a thermal conductivity measurement, in order to have the least self heating effect when reading the resistance of thermal sensors, we would set the lowest possible excitation voltage for sensors, without losing the precision of our resistance reading. In our experiment the two thermal sensors are read first, followed by reading the resistance of a reference sensor. As the reference sensor is connected to the copper block and is not in direct connection with the other two sensors, self heating issue in these sensors can not affect the reference significantly. Therefore, one could

set the optimal excitation voltage for these sensors independent of the effect that it might have on the reference thermometer. In order to find the optimal voltage, one could start with a random value and then if by decreasing the voltage the average of the resistance of the sensors goes up, it means that there is some self heating in the system, so one could pick up a lower voltage and this algorithm continues. However if by setting a lower voltage, the average reading of the resistance does not change and the only difference is that reading becomes noisier then, this would be a sign of having the optimal excitation voltage. Fig.3.8 shows the result of setting three different voltages for one of the thermal sensors.

2) In order to see if the resistance of the contacts on the sample is too high comparing to sample itself, one can monitor the resistance of the hot sensor simultaneously when the excitation voltage which is used for reading the resistance of the sample is being changed. Normally the resistance of the sensor is very small and should not change by changing the measuring voltage. Therefore if by changing the voltage, the resistance of the hot sensor changes, one can understand it as an effect of the resistance of the contacts.

## 3.6 Thermometry issues

One of the most important issues in measuring thermal conductivity at very low temperatures is the accuracy of thermometry. On the cryostat used in our measurements, the 1K pot which provides the cooling power is in thermal contact with a brass block through a 0.5 cm long stainless steel tube and the thermometer and heater of the temperature controller are mounted inside the brass block. Attached to the brass block is a copper piece where current and voltage leads are mounted in and is in direct thermal contact with the sample holder and reference sensor. Fig.3.9 is a close–up of this part of the cryostat.

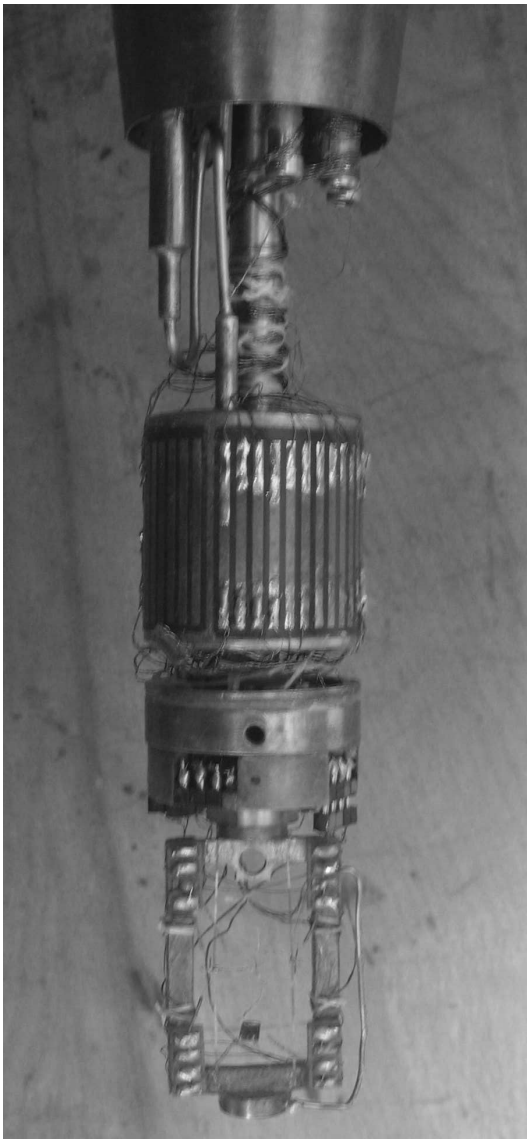

Figure 3.9: A close–up of sample holder along with 1K pot

One of the very first problems in measuring the temperature of the sample holder was the existence of a distinct difference in temperature between the mount and the temperature control sensor mounted on the 1K pot. Furthermore the temperature gradient between these two points varied as a function of helium level in the 1K pot. Although we do not know the exact origin of this problem, we speculate that it might be due to the proximity of the temperature sensor in regard to the heater. To solve the problem we introduced a second calibrated sensor that we call the reference thermometer and was located directly on the thermal conductivity mount and connected to the same point as the sample. Since this reference thermometer was used to directly measure the temperature of the sample, it avoids the variable temperature gradient problem and the temperature control sensor was simply used to maintain a stable temperature at approximately the temperature at which the measurement was to be made.

Another problem was the sensitivity of our thermometry to the vibration. As mentioned for reducing the temperature one needs to pump on $^4He$ and the pumping line which was a series of flexible pipes, would transfer a significant level of vibration to the cryostat. This vibration would affect the thermal sensors which were suspended on the kapton ribbons more than the reference thermometer which was mounted to the copper frame. The effect of vibration on the readings of resistance could be seen by using an oscilloscope connected to the preamplifier output of the resistance bridge. In order to damp the vibration along the pumping line, we put a heavy lead block on the pipes in between the pump and the valves on the cryostat. This would reduce the vibration very effectively and the level of noise on the oscilloscope showed a remarkable decrease.

In order to obtain a low noise temperature reading, one needs to average several data points. The process of averaging the collected data points was done twice, once by the resistance bridge we used for reading the resistance of temperature sensors and a second time by the LabView program which acted as an interface between the

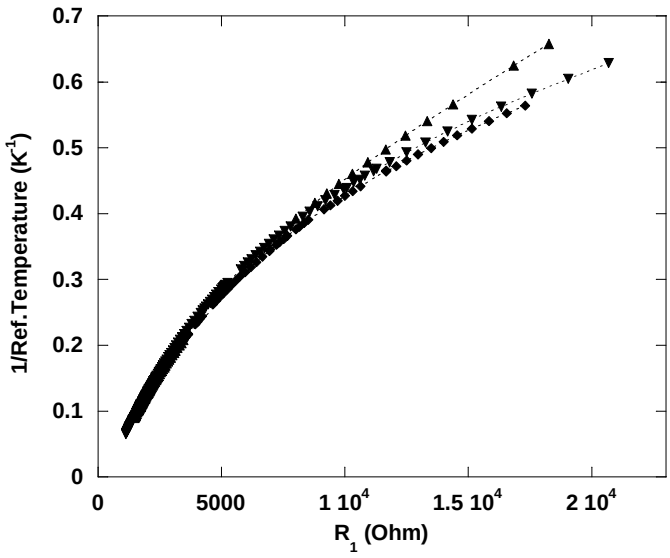


Figure 3.10: Having different calibration curve can be a result of a bad thermal joints

bridge and computer. The averaging process done by the resistance bridge could be controlled by a digital filter option. By setting the bridge with a specific digital filter, the bridge would spend that time to collect data and the output of the bridge was the average of those data points. "N" of these data points were collected by the LabView program and averaged to make the final data recorded by the program. One could change the level of noise in the data recorded by setting different digital filters or enforcing different values of "N". Therefore one of the challenges we faced for doing and accurate thermometry was to find the optimal values for the digital filter and number of data points to be collected. Usually the longer it takes to collet the data, the more accurate they are, but the measurements can become cumbersome. A final challenge to having accurate thermometry is to have good

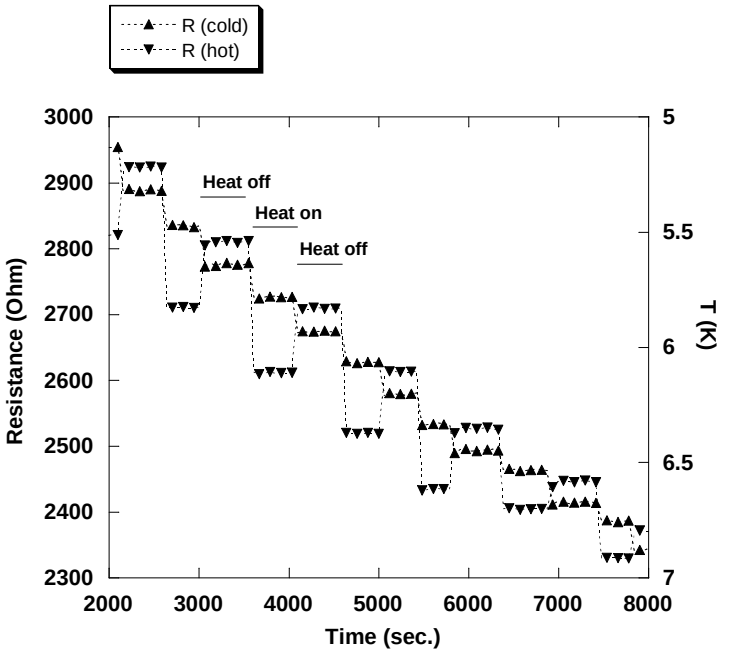


Figure 3.11: Resistance of hot and cold sensors as a function of time, during heat off and on periods

thermal contacts between the sample and the temperature sensors, so that one could get the least temperature gradient between the sample and each sensor. For the same reasoning that was explained in the self heating section, having a bad thermal contact can give rise to getting different calibration curves for a sensor at the same temperature range. Fig.3.10 displays three different calibration curves for one of the temperature sensors as results of having a bad joints between that sensor and the sample. The best curve would be the one that has the highest resistance at a particular temperature.

## 3.7 Experimental procedure

The experiment is directed by an interactive program written with the "LabVIEW" software. For each point, once the temperature of the kappa mount is adjusted by the temperature controller, we waited to reach equilibrium in all three sensors and the sample. The setup is considered to be in the thermal equilibrium, when $\frac{R_{max}-R_{min}}{R_{avg}}$, where $R_{max}$, $R_{min}$ and $R_{avg}$ are the maximum and minimum and average values of the N last data points, of both thermal sensors and the reference sensor , is below a value that could be called the tolerance for making an accurate measurement. The tolerance and N are enforced by the user and stored in the program. At this stage the temperature of the controller thermometer and the resistance of both thermal and reference sensors $R_{hot}(\dot{Q}=0)$, $R_{cold}(\dot{Q}=0)$ and $R_{ref}(\dot{Q}=0)$, are averaged and then recorded. $\dot{Q}$ stands for the power of the heater which at this point is off. This data is needed to calibrate the thermometers. Then the heat is applied to the sample. $\dot{Q}$ must be set in a way that the temperature gradient across the sample stays less than 10 % and more than 5 % of the temperature that the set up is at. The reason is that we used the assumption of having a linear temperature gradient across the sample. However unless the sample has constant thermal conductivity with temperature this will not be true and is therefore only an approximation which is close to the real situation for small variations in temperature across the sample and hence small variations in conductivity. The reason of keeping this ratio above 5 % is to make sure that the noise is not significant relative to the measured signal. So it is crucial to keep the $\frac{\Delta T}{T} < 0.1$ condition valid while measuring thermal conductivity. By assuming the thermal conductivity will be linear at low temperatures, one can find the output power of the heater and knowing $\dot{Q} = \frac{V^2}{R_{heater}}$, the appropriate voltage needed to be applied to the heater can be found. After the system reaches to thermal equilibrium by satisfying the value set by the tolerance numbers, the program records the voltage applied by the heater,

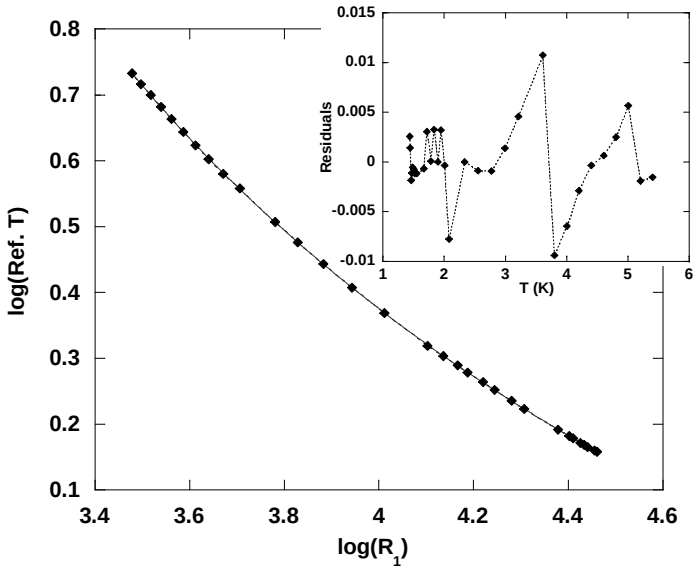


Figure 3.12: Since the longer the temperature range is the less accurate the fit would be, fitting was done in a small temperature range, above is a $5^{th}$ order polynomial fitting, the inset displays the residual of this fit

the new values of thermometers' resistances, $R_{hot}(\dot{Q})$, $R_{cold}(\dot{Q})$ and $R_{ref}(\dot{Q})$ and the temperature of the controller thermometer is checked to see that it has not increased appreciably comparing to the temperature gradient across the sample when the heater is on. By plotting $\log(R_{hot})$ and $\log(R_{cold})$ as a function of $\log(R_{ref})$, when the heat is off, and fitting a polynomial to it, we find the calibration function of the uncalibrated thermal sensors and deduce the temperature of sensors when the heaters are on. Fig.3.11 displays the resistance of the cold and hot sensors as a function of time. The sensor that is affected more by the heat is the hot sensor which is closer to the heater and the other one, the cold sensor is at a distance further away from the heater. By having the geometric factor of the sample, and

measuring the temperature gradient across the known length it one can calculate the thermal conductivity of the sample by using the following relation :

$$\kappa(\overline{T}) = \frac{\dot{Q}}{(T_{hot} - T_{cold})} \times \frac{l}{A}. \tag{3.5}$$

where l and A are the length and the cross section area of the sample and $\overline{T}$, $T_{hot}$ and $T_{cold}$ are the average temperature and temperature of the hot and cold ends of the sample respectively. Fig.3.12 displays the calibration plot and fit function of one of the sensors as a function of temperature. In order to see how well the fit function is, one can look at the residual of the function which shows the difference between the fit function and the data points. The residuals of a good fit function should have a random distribution around zero (inset of fig.3.12).

## 3.8 Test on the silver sample

In order to test our experimental setup, we measured the electrical resistance and the thermal conductance of 1 cm long silver wires of 25 and 50 $\mu$m diameters and of 99.99% purity. The Sommerfeld value divided by the resistivity of the sample, thermal conductivity and Lorenz ratio are plotted in figs.3.13 and 3.14 as a function of temperature. One finds the characteristic features of the transport properties of normal metals at low and intermediate temperatures in these plots as the following :

Below 10 K, electrical resistivity is determined by the effect of the scattering of conduction electrons by impurity ions and since the impurity distribution does not depend on the temperature, the resistivity does not depend on temperature either. At this range and for this level of purity of silver, the electrons have the dominant contribution to thermal conductivity, $\kappa(T) \sim \kappa_e$ and Wiedemann-Franz law holds, so $\frac{\kappa_e \rho}{T} = L_0$ where $L_0 = 2.44 \times 10^{-8}$. The thermal conductivity will have a linear

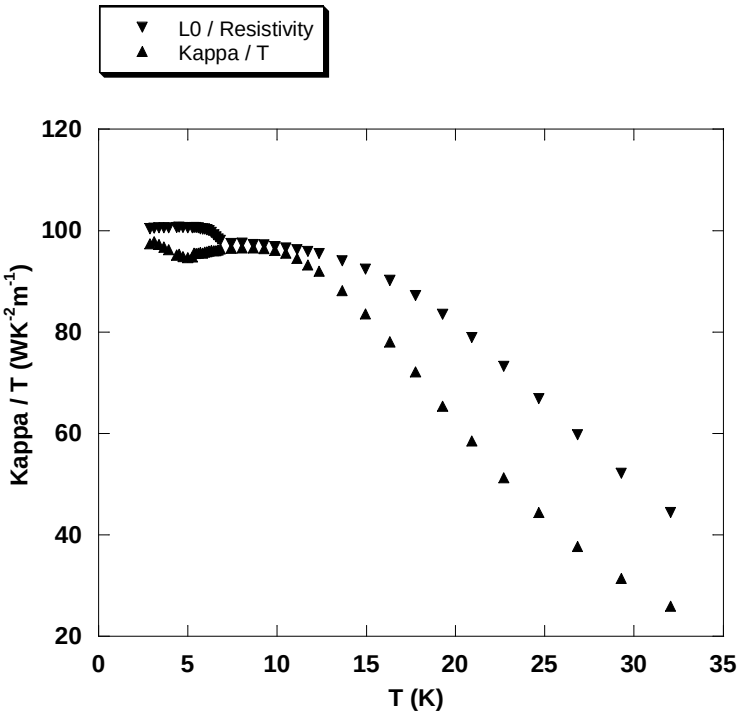


Figure 3.13: Temperature dependence of the Sommerfeld value divided by the resistivity, $\frac{L_0}{\rho}$, and thermal conductivity divided by temperature, $\frac{\kappa}{T}$, for the silver wire. The nature of the step on $\frac{L_0}{\rho}$ at about 7 K is unknown, though it might be due to the effect of tin–lead solder that we used for making the joints on the sample

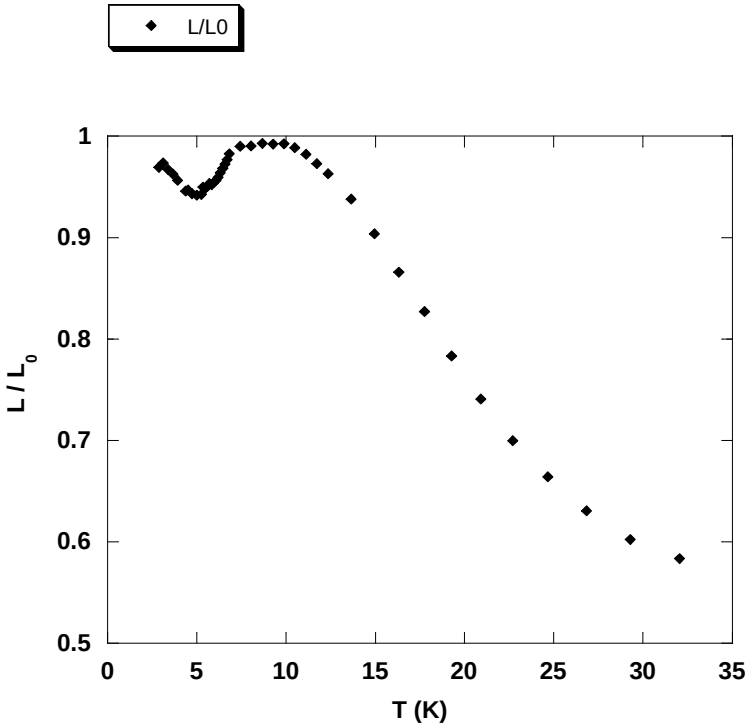


Figure 3.14: Plot of the ratio of experimental Lorenz number to theoretical Lorenz number

temperature dependence and $\kappa(T)/T$, resistivity and Lorenz ratio will display a plateau below 10 K.

Above 10 K as the thermal vibration of the lattice increases, phonons start to take a role in transporting heat and scattering electrons. Two factors will affect thermal conductivity at this point. The number of phonon carriers of heat increases as the temperature increased. This would increase $\kappa(T)$ if the mean free path of phonons stayed constant. In reality since the phonon contribution is very small compared to the electronic conduction, the increase in number of phonons results in the increase in electron–phonon scattering which suppresses $\kappa(T)$. So above

10 K $\kappa(T)$ and $\kappa(T)/T$ will exhibit a decrease with increasing temperature. The Wiedemann-Franz law does not hold at this temperature range and as fig.3.14 displays the $L/L_0$ ratio will decrease with temperature.

At higher temperatures one expects $L/L_0$ to become close to 1 again as the result of the scattering of electrons by high energy phonons. In that range the thermal conductivity will become a constant in temperature and the electrical resistivity increases linearly with temperature and the Lorenz number will be constant.

In conclusion, we recovered the Sommerfeld value of the Lorenz number in the low temperature limit to within 5 %. This is the only region in which we could directly verify the thermal conductivity value we measured. Based on this accuracy, we assume the results are equally accurate up to temperatures of at least 30 K. This verifies the reliability of our measurement setup and the method we used for doing our measurements.

# Chapter 4

# Experimental review

The filled skutterudite compounds are known with the general formula $ReTr_4Pn_{12}$, where Re is a rare earth ion, (Pr, La, Ce), Tr is a transition metal ion, (Fe, Ru, Os) and Pn is a pnictogen atom, (P, As, Sb). The primitive cell has a body centered cubic (BCC) form in which each RE ion is surrounded by twelve Pn atoms and eight Tr ions. The packed BCC structure can give rise to strong hybridization between electrons of f shells of the RE atoms and conduction electrons. Fig.4.1 shows the crystal structure of the filled skutterudites.

## 4.1 Sample growth

In this chapter we will review the properties of two Pr–based skutterudite compounds, $PrRu_4Sb_{12}$ and $PrOs_4Sb_{12}$. Single crystals of these compounds were grown by Brian Maple in UC San Diego, using an Sb flux method. The elements (Ames 99.999% Pr, Colonial Metals 99.95% Os and Ru and Alfa Aesar 99.9999% Sb) were sealed under 150 Torr Ar in a carbon coated quartz tube in the ratio 1:4–4x:4x:20, heated to 1050 C at 50 C/h, then cooled at 2 C/h to 700 C. The samples were

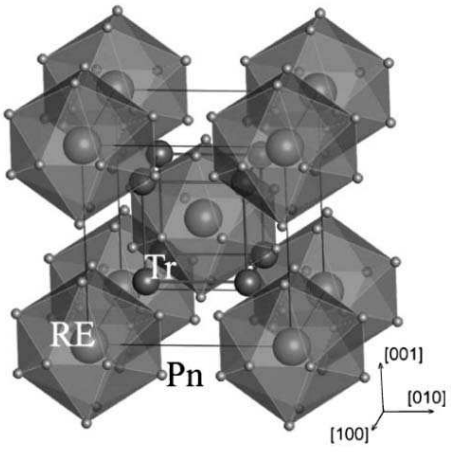


Figure 4.1: Cubic Structure of skutterudite compounds [27]

then removed from the furnace and the excess Sb was spun off in a centrifuge. the crystals were removed from the leftover flux by etching with dilute aqua regia ($HCl : HNO_3 : H_3O = 1 : 3 : 3$) [17].

## 4.2 $PrRu_4Sb_{12}$

$PrRu_4Sb_{12}$ is a metallic compound that become superconducting below $T_c = 1.1$ K. The lattice constant of this compound is reported 9.27 $\mathring{A}$ which is the smallest value in compounds with general formula $Pr(Os_{1-x}Ru_x)_4Sb_{12}$ [17]. In the normal state the transport properties of this compound is very similar to that of regular metallic compounds.

The electrical resistivity shows no anomalies and decreases with decreasing temperature.

The magnetic susceptibility follows a Curie–Weiss law down to 50 K and becomes constant at lower temperatures. The effective paramagnetic moment was

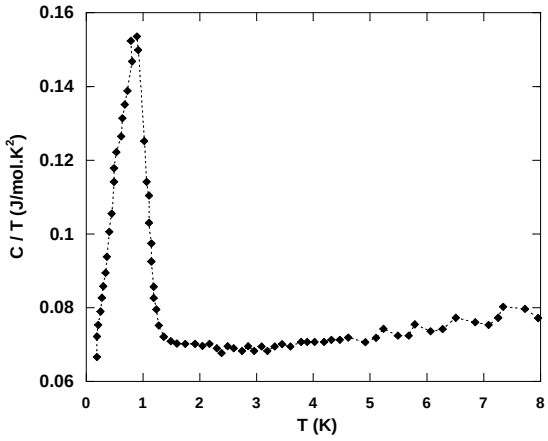


Figure 4.2: Temperature dependence of specific heat of $PrRu_4Sb_{12}$ [20]

reported $\mu_{eff} \sim 3.58\mu_B$ which is close to $3.44\mu_B$ of free $Pr^{3+}$ ions. The absence of any magnetic transition at lower temperatures implies that $PrRu_4Sb_{12}$ is a paramagnet with a singlet ground state [20]. The measurements of transport and magnetic properties also imply the absence of hybridizations between the conduction a f electrons [18–20].

The specific heat decreases with reducing the temperature and displays a jump at $T_c$. Fig.4.2 displays the superconducting transition in specific heat of $PrRu_4Sb_{12}$ reported in [20]. The specific heat measurements shows a jump at $T_c$ with an electronic coefficient of about $\gamma = 59\ mJ/mol.K^2$ [20, 21]. The $\gamma$ value and the jump of specific heat at $T_c$ gives the ratio $\Delta C/\gamma T_c$ to be 1.49 which is very close to 1.43 for conventional superconductors and suggests a weak coupling between the electrons that is mediated by phonons which could give rise to an isotropic superconducting gap. Besides the Specific heat measurements, measuring superfluid density exhibits exponential behavior at low temperatures and an energy gap of the order of $2\Delta = 3k_BT$ [22].

## 4.3 $PrOs_4Sb_{12}$

$PrOs_4Sb_{12}$ is the first Pr–based skutterudite showing properties of a heavy fermion state in the normal state with an effective mass of the order of $50m_e$. It has the largest lattice constant, $\sim$ 9.30 $\mathring{A}$ among compounds with general formula $Pr(Os_{1-x}Ru_x)_4Sb_{12}$ [17].

The resistivity of this compound decreases with reducing the temperature and goes to zero at about 1.81 K. The "roll–off" feature observed about 8 K can be explained based on crystalline electric field effects. It will be discussed later that the crystalline electric field Hamiltonian can be made based on both magnetic exchange and aspherical coulomb scattering. Fermi liquid behavior in resistivity can be seen above 8 K. Under large enough magnetic fields the Fermi liquid behavior can be observed below 8 K with a large A coefficient of about 1.4 $\mu\Omega cm/K^2$ [27].

The thermal conductivity measurements in zero magnetic field display a decrease and an increase below $T_c$ [23, 34]. The angle resolved magneto-thermal conductivity measurements show two distinct superconducting states with different nodal structures. Fig.4.3 shows the evolution of the nodal structure with magnetic field reported in [23]. Fig.5.10 in chapter 5 exhibits the phase diagram proposed in [23]. In contrast to the angle resolved magneto-thermal conductivity measurements that bring up the possibility of nodes on the energy gap, experiments on muon spin rotation and a $T^2$ temperature dependent penetration depth is consistent with the assumption of an isotropic superconducting gap [27].

The specific heat measurements of this compound which so far has been very sample dependent exhibit a double jump at and below $T_c$. Some measurements show the absence of the second jump which occurs below $T_c$ [25]. The jump of specific heat at $T_c$ is reported $\Delta C/T_c \sim 500\ mJ/mol.K^2$. The value of electronic specific heat coefficient from the weak coupling BCS prediction $\Delta C/\gamma T_c = 1.43$ is $\gamma \sim 350\ mJ/mol.K^2$, where from experiments $\gamma \sim 750\ mJ/mol.K^2$ is obtained [19], which

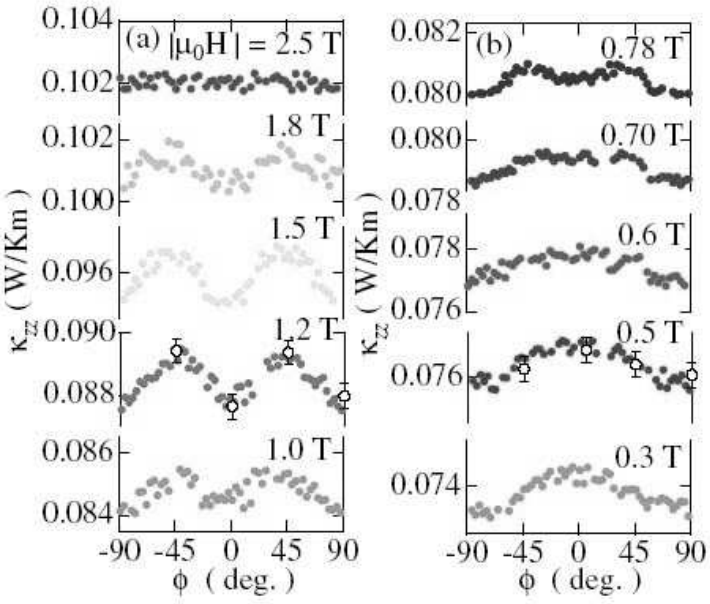


Figure 4.3: The field dependent evolution of phase structure of $PrOs_4Sb_{12}$ [23]

suggests the strong coupling between electrons. The presence of a double jump in specific heat at $T_c$ and right below $T_c$ has also strengthened the assumption of a double phase superconducting state like the one observed in $UPt_3$.

An ordered phase has been observed under magnetic fields $> 4.5$ T and temperatures $< 1.5$ K. This ordered phase might have either a magnetic or a quadrupolar origin suggesting that the superconductivity might occur in the vicinity of a quantum critical point [27].

In the following chapters we will discuss the results of measurements on transport properties of single crystals of $PrRu_4Sb_{12}$ and $PrOs_4Sb_{12}$, and investigate the effect of crystalline electric field on these compounds.

# Chapter 5

# Transport properties of $PrOs_4Sb_{12}$

We did thermal and charge conductivity measurements on two single crystal samples of $PrOs_4Sb_{12}$. The direction of thermal current in all cases was in the same direction as one of the main axes of crystals which have cubic symmetry. The superconducting transition temperature of both samples was measured to be 1.81 K. All measurements were done in zero magnetic field and in a $^4He$ cryostat. Since we used an AC current for measuring the electrical resistivity of this compound, any possible thermal current that was generated in the sample, would average to zero. Thus the thermo-electric properties, that are known to be large in this material, do not affect the results of the measurements of the electrical resistance. In this chapter the results of heat and charge conductivities of two $PrOs_4Sb_{12}$ samples will be discussed.

## 5.1 Electrical resistivity of $PrOs_4Sb_{12}$

Resistivity of the $PrOs_4Sb_{12}$ samples were measured between room temperature and 1.45 K for the sample A and 1.1 K for sample B. We were able to extend the

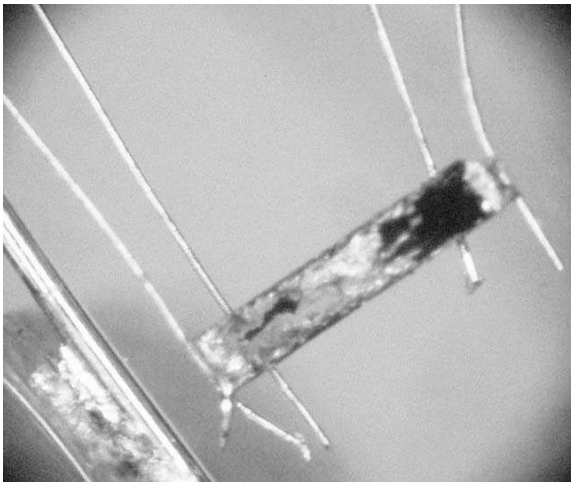

Figure 5.1: First sample of $PrOs_4Sb_{12}$. Geometric factor, $l/A$ used for sample A was 7630

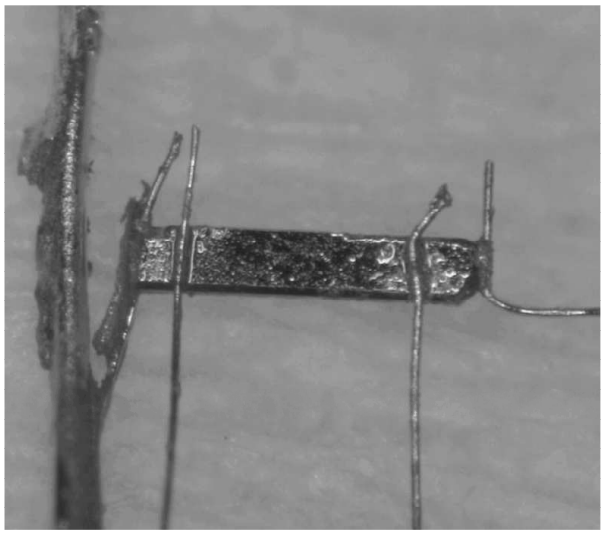

Figure 5.2: Second sample of $PrOs_4Sb_{12}$. Geometric factor, $l/A$ used for sample B was 40323

temperature range of the measurement on sample B by extending the calibration range of our temperature controlling sensor. Therefore the lowest temperature at which the electrical resistance of sample B was measured, was 1.1 K. Dimensions of sample A were $785 \times 200 \times 330 \mu m$ and those of sample B were $1080 \times 185 \times 100 \mu m$ where in both cases the direction of the thermal and electrical currents were in the direction of the longest dimension. Fig.5.3 compares the resistivity of the samples of our experiments and the resistivity data published in [28] as a function of temperature. A good agreement was observed in qualitative temperature dependence of all three sets of data. Although the plots are quantitatively a bit different in the whole range which might be an indication of different purity levels, the superconducting transition occurs exactly at the same temperature for all samples. The width of transition is $\Delta = 0.28K$ and $T_c$ is defined as the midpoint of the drop in the resistivity. The resistivity of sample B at room temperature (293K) was found to be $150 \mu\Omega$cm and the resistivity slightly above $T_c$ was 4.6 $\mu\Omega$cm, therefore the residual resistivity ratio, RRR, which is defined as $\frac{\rho(293K)}{\rho(2K)}$, will be about 33 compared to 30 and 40 reported in [28] and [29] respectively. Since the room temperature resistivity is determined mainly by thermal vibrational scattering and the low temperature resistivity is affected by impurity scattering, the high RRR value can be an indication of the high purity level of a sample. The impurities are associated with excess Sb due to the Sb flux method in which the crystals are grown. This type of impurities are believed to be nonmagnetic and so does not have any kind of magnetic interactions with the conduction electrons.

We observed a qualitative metallic behavior in electrical resistivity which is a decrease in resistivity as the temperature is reduced. Although one could notice an exotic feature in resistivity of $PrOs_4Sb_{12}$ that is manifested as a "roll-off" at 8K. It has been shown that this feature can be explained based on both magnetic exchange and aspherical coloumb scattering. This change in the curvature, from negative to positive is consistent with a decrease in the scattering of the conduction electrons

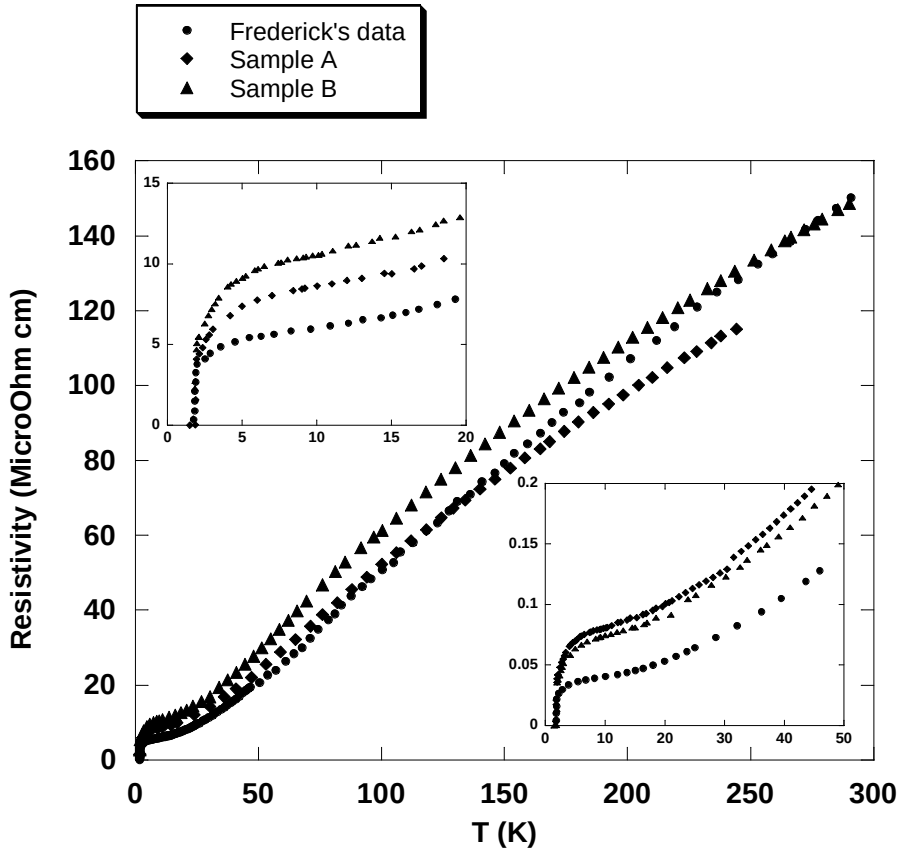


Figure 5.3: Temperature dependence of the electrical resistivity of both $PrOs_4Sb_{12}$ samples compared with the data reported in [28], the upper inset shows the low temperature behavior, where one notices that the samples have the same $T_c$'s and the lower inset is the temperature dependence of $\frac{R(T)}{R(245K)}$

by $Pr^{3+}$ ions due to a decrease in the population of the first excited state of the crystal electric field spectrum (CEF) separated from the ground state by about 7 K [26]. The total contribution of CEF effects to the resistivity can be expressed as,

$$\rho_{CEF} = \rho_0[rTr(PQ^M) + (1-r)Tr(PQ^A)], \tag{5.1}$$

where r is the coefficient representing the ratio of the magnetic exchange term to the coloumb scattering term [28]. $P_{ij}$ is the temperature dependent matrix and its elements can be expressed as,

$$P_{ij} = \frac{\exp(-\beta E_i)}{\sum_k \exp(-\beta E_k)} \frac{\beta(E_i - E_j)}{1 - \exp(\beta(E_i - E_j))}, \tag{5.2}$$

where $E_i$'s are the eigenvalues of the CEF eigenstates and $\beta = 1/k_BT$. The CEF Hamiltonian is given by,

$$H = W(x(O_4/60) + (1-|x|)(O_6/1260)), \tag{5.3}$$

where W and x are the parameters that can be chosen in accordance with the LLW formalism [32] and $O_4$ and $O_6$ are given by the following relations,

$$\begin{aligned}
O_4 &= 35J_z^4 - (30J(J+1) - 25)J_z^2 - 6J(J+1) \\
&+ 3J^2(J+1)^2 + \frac{5}{2}(J_+^4 + J_-^4), \\
O_6 &= 231J_z^6 - 105(3J(J+1) - 7)J_z^4 \\
&+ (105J^2(J+1)^2 - 525J(J+1) + 294)J_z^2 \\
&- 5J^3(J+1)^3 + 40J^2(J+1)^2 - 60J(J+1) \\
&- \frac{21}{4}(11J_z^2 - J(J+1) - 38)(J_+^4 + J_-^4) \\
&+ \frac{1}{4}(J_+^4 + J_-^4)(11J_z^2 - J(J+1) - 38).
\end{aligned}$$

The $Q^M$ and $Q^A$ represent magnetic exchange scattering and coloumb scattering due to the quadrupolar charge distribution of $Pr^{3+}$ ions and their elements are

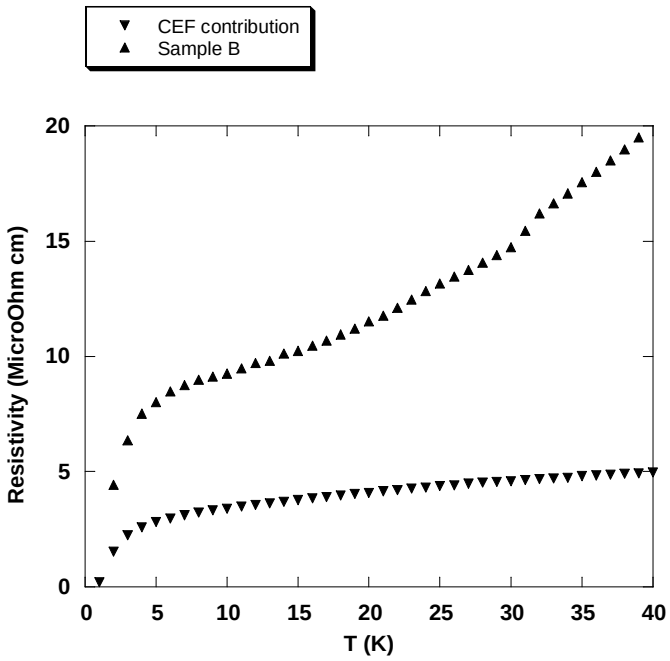


Figure 5.4: Electrical resistivity versus temperature between 1 and 40 K of sample B along with the CEF contribution to the resistivity for which $W = -2.78$, $x = -0.720$, $\rho = 0.378\mu\Omega cm$ and $r = 0.25$ [28]

given by [30], [31] :

$$Q_{ij}^{M} = |\langle i|J_z|j\rangle|^2 + \frac{1}{2}|\langle i|J_+|j\rangle|^2 + \frac{1}{2}|\langle i|J_-|j\rangle|^2, \tag{5.4}$$

$$Q_{ij}^{A} = \sum_{m=-2}^{2} |\langle i|y_2^m|j\rangle|. \tag{5.5}$$

where $|i\rangle$'s are the CEF eigenstates and $y_2^m$ are the operator equivalents of the spherical harmonics for $L = 2$ that can be found in [33].

The $Q_{ij}$–matrices are normalized to each other, such that $\sum_{i,j=0}^{n} Q_{ij} = 180$ for both interactions. Using MATLAB we calculated the CEF contribution to the total resistivity. Fig.5.4 shows the CEF contribution to the resistivity of a cubic

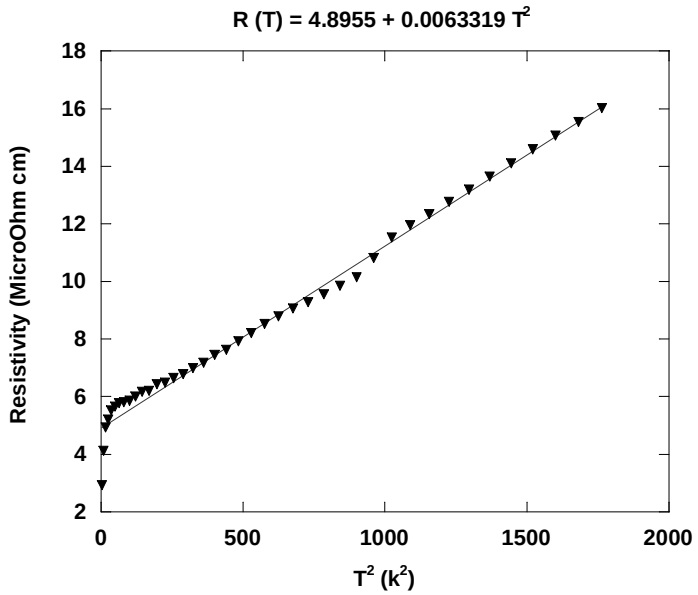


Figure 5.5: Electrical resistivity of $PrOs_4Sb_{12}$ at 8–40 K fits very well with a Fermi liquid expression of the form $\alpha + \beta T^2$

crystal. According to Matthieson's rule, the electrical resistivity can be separated into the scattering of electrons by impurities, other electrons, the lattice vibration and the contribution of CEF effects.

$$\rho(T) = \rho_{imp} + \rho_{e-e} + \rho_{CEF} + \rho_{e-g}. \tag{5.6}$$

Having a look at fig.5.4, one could notice that above 25 K when the CEF effect saturates, the resistivity still has a temperature dependence which implies there must be another scattering mechanism affecting the conduction electrons. After subtracting the CEF contribution from the total resistivity, the temperature dependence of the remaining part fits very well with a $\rho_{imp} + \beta T^2$ function. The

electrical resistivity rising up by e–e scattering has also a $T^2$ form, so that part of resistivity that is not coming from CEF effect, could be the effect of electron–electron scattering. Fig.5.5 displays the fit function done on the resistivity of sample B. The coefficient of the second order term is 0.006 $\mu\Omega\text{cm}K^{-2}$ which is close to 0.009 $\mu\Omega\text{cm}K^2$ reported in [28]. This type of behavior is consistent with the Fermi liquid behavior. The kink at 35 K in the plot might be the result of attaching two different sets of data. The highest temperature at which we took the resistivity in a temperature controlling way is 32 K and the resistivity at higher temperatures is taken from the cooling down curves which were not temperature controlled. Above 40 K, the resistivity due to the scattering of electrons by phonons, $\rho_{e-g}$, is believed to be the dominant term.

Having set these results, we showed that the change in the curvature of the resistivity at 8 K can be explained based on the crystalline electric field's effect, and the Fermi liquid behavior can be observed in 8–40 K range. The effect of phonons on scattering electrons is believed to be remarkable above 40 K.

## 5.2 Thermal conductivity of $PrOs_4Sb_{12}$

Temperature dependence of the thermal conductivity of $PrOs_4Sb_{12}$ samples was measured in 1.1K–40K range. Fig.5.6 displays temperature dependence of thermal conductivity divided by temperature, $\kappa(T)/T$ for both samples. Both samples show similar features and as the temperature is reduced, $\kappa(T)/T$ increases to make a maximum at 14 K. At 4–14 K range it comes down monotonically to take a minimum at 4 K which is 0.9 of the maximum at 14 K for sample A and 0.83 of the maximum value at 14 K for sample B. Upon entering the superconducting state $\kappa(T)/T$ is suppressed again to take a minimum at 1.6 K followed by another maximum at 0.8 K which has the highest value comparing to the other two maximums.

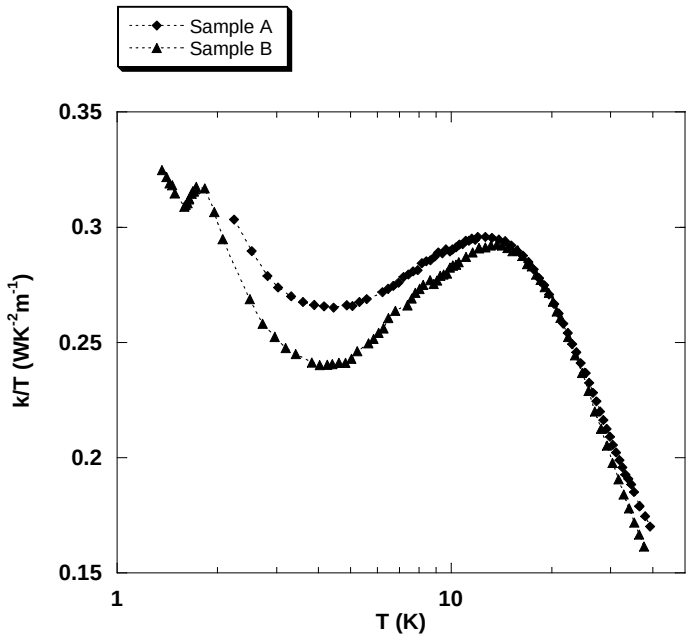


Figure 5.6: Thermal conductivity of two $PrOs_4Sb_{12}$ samples as a function of temperature

We believe both electrons and phonons play a role in determining the unusual temperature dependence that is observed in the thermal conductivity of this compound. In the following sections we try to explain these extremums and their origins.

### 5.2.1 Thermal conductivity in the normal state, $T = 1.81 - -40K$

It was observed in $\kappa(T)$ of silver that as the temperature is reduced below 50 K, thermal conductivity increases. Since the number of phonons and the lattice thermal conductivity decrease with reducing the temperature one can see that the

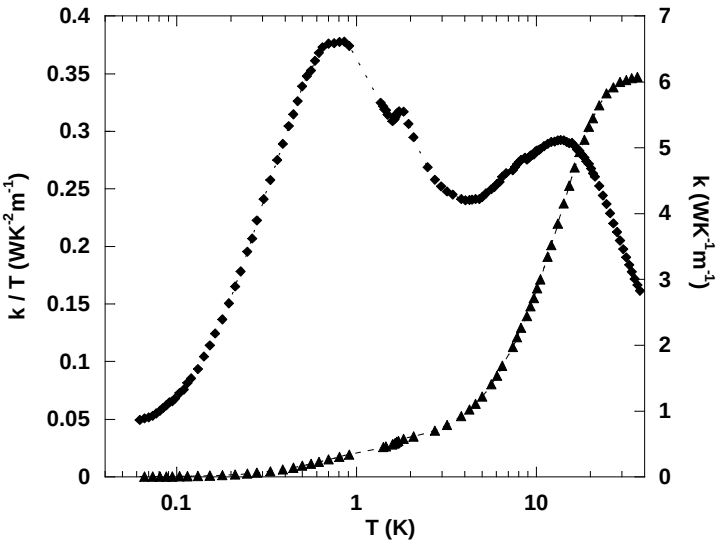


Figure 5.7: Temperature dependence of $\kappa(T)$ and $\kappa(T)/T$ of sample B. The experiment below 1 K was performed by Rob Hill with a dilution refrigerator in the department of Physics, University of Sherbrooke [40]

electronic contribution to the heat transport will become more pronounced at this temperature range. The increase in $\kappa(T)$ which is due to the decrease in electron–phonon scattering would be suppressed by electron–impurity scattering that is the dominant scattering mechanism at very low temperature. Therefore the resultant maximum in $\kappa(T)$ below 20 K has electronic nature. Fig.5.7 exhibits the thermal conductivity $\kappa(T)$ and $\kappa(T)/T$ of sample B versus temperature. Contrary to the thermal conductivity of the silver, $\kappa(T)$ of $PrOs_4Sb_{12}$ is decreasing in the whole measurements range. The maximum and the minimum at 14 K and 4 K on $\kappa(T)/T$ occur at the same temperature range that $\kappa(T)$ has a steep slope. In the following section we will consider the possible phononic and electronic origins for these

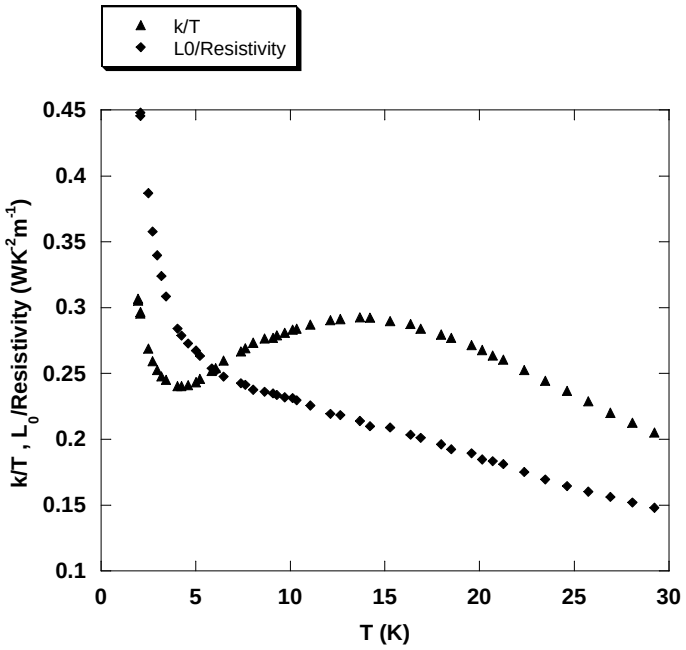


Figure 5.8: $\kappa/T$ and $L_0/\rho$ of sample B of $PrOs_4Sb_{12}$ as a function of temperature, The "roll-up" feature happens at a similar temperature that the minimum in $\kappa(T)/T$ comes up

extremums and provide a qualitative description of the data based on reasonable expectations for the temperature dependence.

### Lattice thermal conductivity

One way to make an estimation of the lattice thermal conductivity is to find an approximation of the electronic thermal conductivity and subtract it from the total thermal conductivity. One can use WF law to make a rough approximation of the electronic part. We will assume that WF law is valid above 10 K and this assumption seems consistent with what is reported in [34]. Fig.5.8 exhibits the temperature

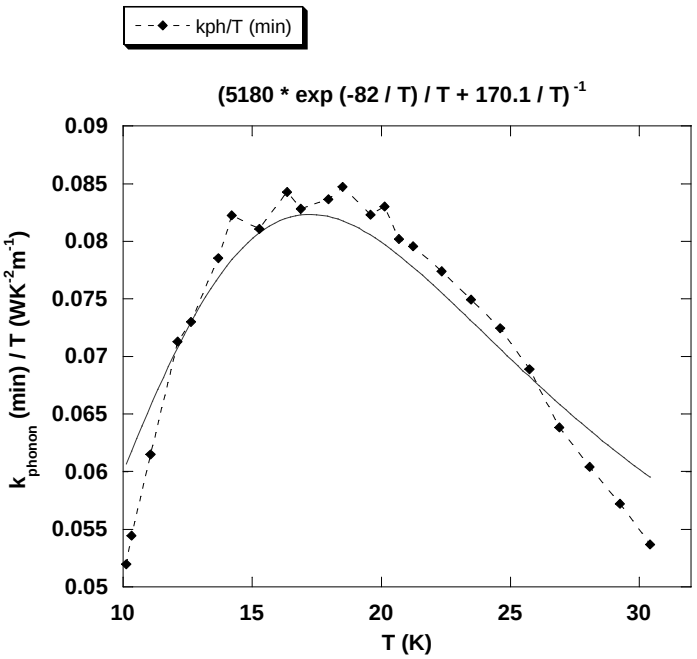


Figure 5.9: Peak at 14 K can still be observed in the minimum contribution of the lattice to the heat transport, the fitting is done with MATLAB

dependence of $L_0/\rho(T)$ which can be considered as the maximum electronic contribution to the heat transport. By having an estimation of the maximum electronic conductivity, the minimum thermal conductivity of the lattice is $\kappa_{total}/T - L_0/\rho(T)$. Fig.5.9 displays the temperature dependence of this minimum lattice conductivity and one can see that this function takes a maximum at the same temperature that the total measured thermal conductivity has a maximum.

On the other hand, in order to have a more quantitative description of this maximum one can see that this maximum can be generated just by taking the phononic thermal conductivity into account. As mentioned in the chapter on the theoretical review, the conductivity of the lattice can be affected by Umklapp process at intermediate and high temperatures and scattering by conduction electrons

and boundaries of the specimen at lower temperatures. The temperature dependence of the umklapp process can be expressed as: $\kappa_u = aT^2 \exp(\Theta_D/bT)$, where a, b are constants and $\Theta_D$ is the Debye temperature which is reported 165 K for $PrOs_4Sb_{12}$ [26].

One can see that as the temperature is reduced, the effect of umklapp process becomes weaker, so $\kappa_u$ increases with decreasing the temperature. However at lower temperatures, scattering of phonons by conduction electrons takes the place of umklapp process and suppresses the lattice conductivity. The thermal conductivity of phonons scattered by conduction electrons can be written as $\kappa_{g-e} = cT^2$, where c is a constant. By using a combination of these two processes and finding the appropriate constants we could simulate the peak at 14 K.

$$\kappa_g = (5180\frac{\exp(\frac{-82}{T})}{T} + \frac{170.1}{T})^{-1}. \tag{5.7}$$

On the other hand one can test the idea of an electronic origin for the maximum at 14 K. The most important mechanisms for scattering electrons at low temperatures are phonons and impurities. The electronic heat conductivity due to scattering of electrons by phonons can be expressed as $T^{-2}$ which increases as the temperature is reduced and in case the scattering mechanism is impurities, it has a linear temperature dependence. A combination of these terms can not be sufficient for explaining the behavior of $\kappa(T)/T$ around 14 K. As it is seen on fig.5.8 there is no features in $L_0/\rho(T)$ which is an estimation of the electronic heat conductivity about 14 K. However the existence of the first minimum on $\kappa(T)/T$ at 4 K, can be linked to the electrons. The "roll-off" feature in resistivity which appears as a "roll-up" in $L_0/\rho(T)$ happens at a similar temperature range that $\kappa(T)/T$ takes its minimum. Even though the Lorenz number may be temperature dependent, if charge conductivity is increasing due to a decrease in scattering of conduction electrons by the $Pr^{3+}$ ions as mentioned in electrical resistivity section, the electronic thermal conductivity would have an increase due to the same reason.

### 5.2.2 Thermal conductivity in the superconducting state ($T < 1.81K$)

At 1.81 K, upon entering to the superconducting state, $\kappa(T)/T$ decreases down to 1.6 K where it turns up to make a maximum at 0.8 K which has the highest value 0.38 $WK^{-2}m^{-1}$, comparing to the other two maximums, 0.29 $WK^{-2}m^{-1}$ and 0.32 $WK^{-2}m^{-1}$ at 13 K and $T_c$ respectively, (the data below 1 K is provided just for sample B). In order to find the origin of the extremums in the superconducting state, we will make an estimation of the lattice thermal conductivity and compare it to the total conductivity.

### 5.2.3 Lattice thermal conductivity

The phonon conductivity in the superconducting state can be estimated in the boundary scattering limit, which provides an upper bound for the phonon thermal conductivity. By using the kinetic formula $\kappa_g = \frac{1}{3}C_g v l$, where $C_g$ is the phonon specific heat, $v = 2000m/s$ [35] and l are the average sound velocity and phonon mean free path respectively and are temperature independent. $C_g$ has a temperature dependence of the form $3.95T^3 mJmol^{-1}K^{-4}$ [26] and l can be considered as the longest dimension of the crystal, so the phonon thermal conductivity could be expressed as $\kappa_g/T = 8T^2 mWK^{-2}m^{-1}$ below 2 K, which is negligible comparing to the total $\kappa/T$. It might suggest that electrons has the dominant contribution to the heat transport in the superconducting state.

### 5.2.4 Electronic thermal conductivity

The extremums of $\kappa(T)/T$ below 1.8 K can be explained based on the decrease in the population of normal electrons which are the main heat carriers at this temperature

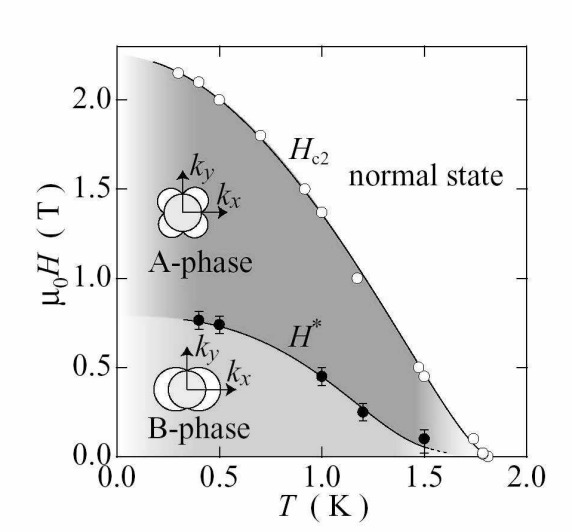


Figure 5.10: Phase diagram of the superconducting gap symmetry proposed by Izawa et. al. in [23]

range and a decrease in the number of electron–electron interactions at the same time. As the temperature is reduced below 1.8 K, when more electrons go to the superconducting state, the electronic thermal conductivity decreases at first which makes a minimum at 1.6 K, by reducing the temperature below 1.6 K, assuming the electron–electron collision is the main scattering mechanism against electron, the increase in the mean free path of the normal electrons will increase $\kappa(T)/T$ until it is limited at about 0.8 K by impurity scattering. Below this temperature, the decrease in the number of electrons as they continue to condense will reduce $\kappa(T)/T$.

To explain the minimum at 1.6 K, one could also consider the possibility of a multiphase superconductivity for $PrOs_4Sb_{12}$. Two distinct observations give rise to the considering the assumption of a multiphase state in this compound.

The first set of experiments was making thermal conductivity measurements in

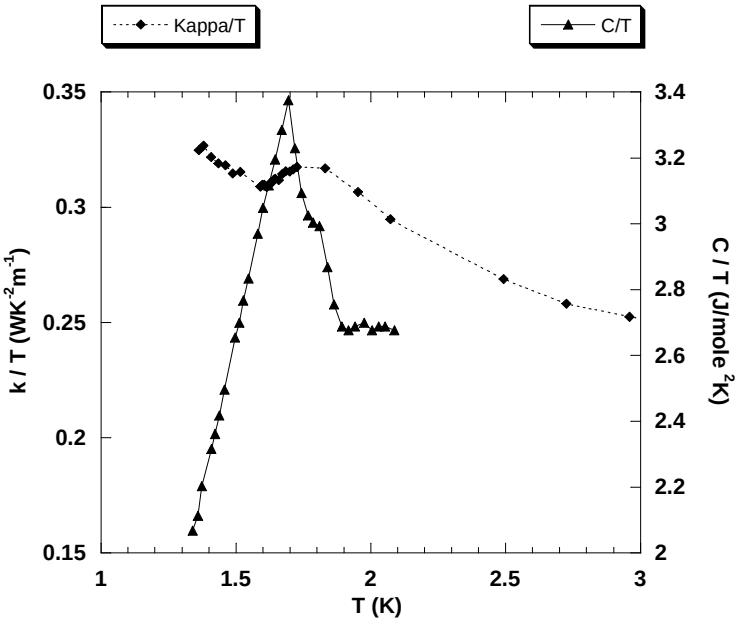


Figure 5.11: Temperature dependence of $\kappa(T)/T$ of sample B and $C(T)/T$ of a $PrOs_4Sb_{12}$ sample from [26] in zero magnetic field

magnetic field which displayed two superconducting phases for $PrOs_4Sb_{12}$, one of them which exists at temperatures above 1.5 K and low magnetic fields has a two fold symmetry and the other one which has a four fold symmetry exists at high magnetic fields and below 1.5 K [23]. Although it is not the only phase diagram proposed for this compound, the general feature of that is in agreement with the other phase diagram suggested in [36].

The second observation was a two level jump observed in the specific heat versus temperature. In zero magnetic field, there is a second order transition in specific heat of the superconducting systems, which is manifested as a jump at $T_c$. For the multiphase superconducting compounds, there would be a multi–level jump. Fig.5.11 shows $\kappa(T)/T$ of sample B and the specific heat divided by the tem-

perature taken from [26]. One could notice that both the maximum of thermal conductivity and the first jump in specific heat occur at 1.8 K, but the minimum of thermal conductivity and the second jump of specific heat are at slightly different temperatures. This might be related to this fact that the specific heat and the thermal conductivity measurements have been done on different samples. By using this fact that the second jump could be related to entering to a new superconducting phase [37], one possibility for explaining the increase in the thermal conductivity below 1.6 K is a transition to a new superconducting state. The change in the gap symmetry could be a way to increase the number of normal electrons and as a result gives rise to an increase in $\kappa(T)/T$. However in order to assure this idea, one needs to do both the specific heat and thermal conductivity measurements on the same sample.

### 5.2.5 Effect of impurities on the thermal conductivity

A discussion has been brought up for explaining the maximum in $\kappa(T)/T$ below $T_c$ in [29], [25] which questions the intrinsic nature of the maximum below 1 K in $\kappa(T)/T$. In this section we will compare the $\kappa(T)/T$ of samples with different purity levels and investigate the effect of the purity of the sample on the extremums in the thermal conductivity.

Using WF law one could say that the more pure the sample is the larger $\kappa(T)/T$ at temperatures slightly above $T_c$ will be. Fig.5.12 displays the comparison between $\kappa(T)/T$ of sample B of the current measurements and sample A and B of [29], where sample B in [29] is reported to be more pure than sample A. $\kappa(T)/T$ of sample B of our measurements is clearly bigger than the other two at temperatures slightly above $T_c$, which is an indication of higher purity level of our sample, which is also approved by comparing the RRR values of these three samples. One could see that even though sample B of our measurements is highly pure, the peak below 1 K is

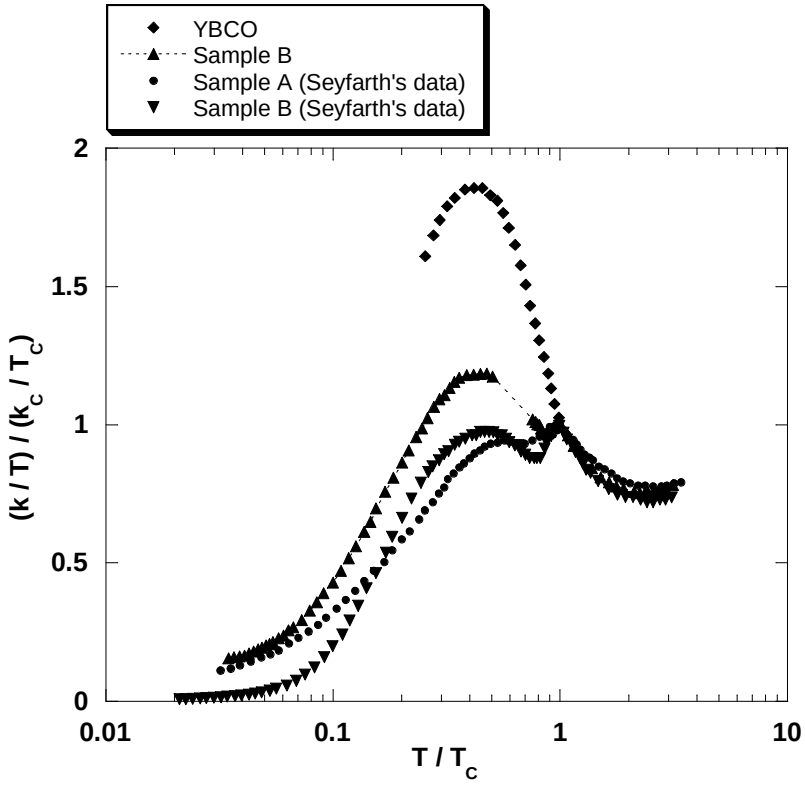


Figure 5.12: Comparison of $\kappa(T)/T$ of three different samples of $PrOs_4Sb_{12}$ with different purity levels and $YBa_2Cu_3O_{7-\delta}$ as a function of temperature

still sharp and clear. This might be an evidence for the intrinsic origin of the peak. In both samples in [29], the peak below $T_c$ is clearly smaller than the peak at $T_c$, which is reversed for our sample. From fig.5.12, it is obvious that sample Bs have a different temperature dependence below 600 mK to that of sample A for which we do not have any explanation at this point.

In order to have a better understanding of the nature of the maximum at 0.8 K, one could make a comparison between $PrOs_4Sb_{12}$ and the high temperature unconventional superconductor $YBa_2Cu_3O_{7-\delta}$. Below its transition temperature

90.5 K, $\kappa(T)/T$ of $YBa_2Cu_3O_{7-\delta}$ takes a maximum which was shown that has electronic origin. It has been discussed broadly in [38,39] that though upon entering the superconducting state the mean free path of phonons increases, as a result of decreasing the number of quasiparticles, but at the same time mean free path of the normal electrons would increase as well. In their discussion they show that the phonon thermal conductivity saturates below $T_c$ and any feature in $\kappa(T)/T$ is a result of changes in the electronic thermal conductivity. Since the Superconducting state in $PrOs_4Sb_{12}$ occurs at much lower temperature where the the lattice thermal conductivity becomes very small, taking into account the correlated nature of both $PrOs_4Sb_{12}$ and $YBa_2Cu_3O_{7-\delta}$, one can expect a similar behavior in the electronic thermal conductivity of these compounds.

### 5.2.6 Nodal structure in the energy gap of $PrOs_4Sb_{12}$

The measurements of thermal conductivity done in the magnetic field show that the field dependence of thermal conductivity is in contrast to that of conventional superconductors [34, 40]. In fact, about 40% of $\kappa$ is restored already at $H \approx 0.07H_{c2}$. For conventional superconductors, small magnetic fields hardly affect thermal conductivity in the low temperature range, in contrast to unconventional superconductors in which small magnetic fields can generate excitations which are big enough for overcoming the energy gap around the nodes. It has been discussed in [34] that the rapid restore of $\kappa(T)/T$ in small magnetic field could be explained by an assumption of a conventional multiband superconducting state, the same thing that occurs in the thermal conductivity of $MgB_2$. Making a comparison between $PrOs_4Sb_{12}$ and some other unconventional superconductors can be useful in having a better understanding of the superconducting state of $PrOs_4Sb_{12}$.

$\kappa(T)/T$ of unconventional superconductors below $T_c$ as a function of temperature behaves in two different ways; it either increases or decreases. In fig.5.13

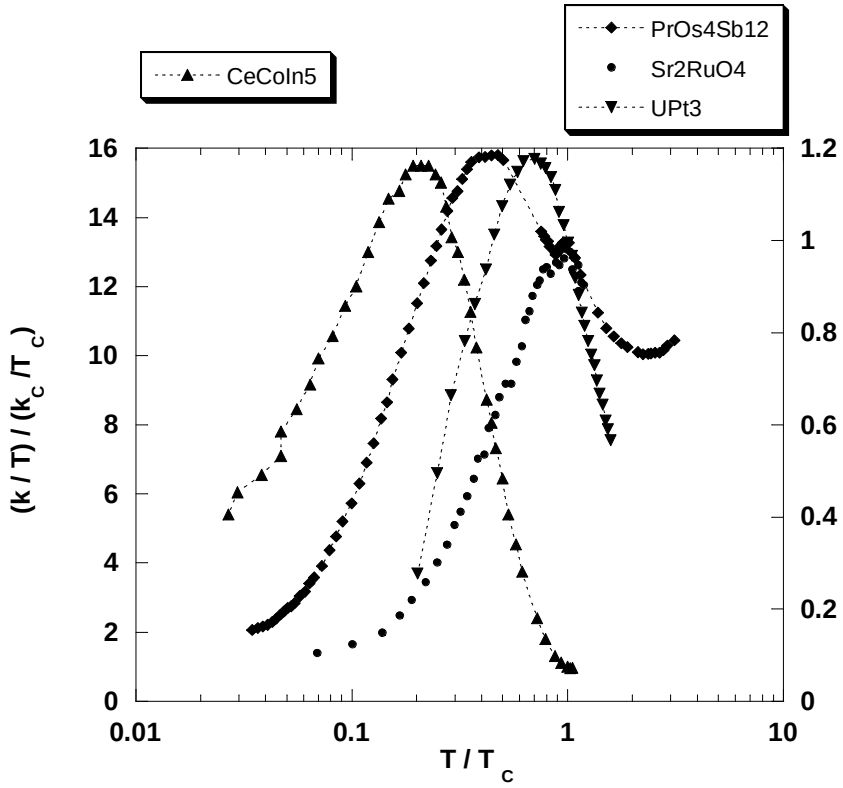


Figure 5.13: Normalized thermal conductivity of $Sr_2RuO_4$, $PrOs_4Sb_{12}$, $CeCoIn_5$ and $UPt_3$ as a function of temperature

$\kappa(T)/T$ of sample B of $PrOs_4Sb_{12}$ along with unconventional superconductors $Sr_2RuO_4$ [41], $CeCoIn_5$ [42] and $UPt_3$ [35] with $T_c$'s 1.5 K, 2.15 K and 0.5 K respectively have been shown. In case of $Sr_2RuO_4$, the linear temperature term in the thermal conductivity decreases below $T_c$ and for the heavy fermion compounds, $UPt_3$ and $CeCoIn_5$, it increases. In the case of $PrOs_4Sb_{12}$ which is also a heavy fermion compound both of these scenarios happen. One could recognize similar behavior in the normalized $\kappa(T)/T$ of these compounds below $T_c$.

It has been discussed broadly that the conductivity of the lattice is negligible

below the transition temperatures of the first three compounds and the electronic part which has a $T^3$ temperature dependence has the dominant contribution. Although further measurements need to be done, in order to know that, this is the right scenario for $PrOs_4Sb_{12}$.

In conclusion, in this section we made an estimation of the electronic and the lattice thermal conductivity of $PrOs_4Sb_{12}$ in the superconducting and normal states. Although further measurements need to be done, the present data shows a small contribution of phonons in the thermal conductivity of the superconducting state while they seem to make the features in the normal state.

# Chapter 6

# Transport properties of $PrRu_4Sb_{12}$

In this chapter we report thermal and charge conductivity results of two single crystal samples of the filled skutterudite compound, $PrRu_4Sb_{12}$. In all thermal conductivity measurements, the direction of thermal current was in the same direction as one of the main axes of crystals which have cubic symmetry. The Wiedemann–Franz (WF) law was investigated in the normal states of the samples. The investigation of transport properties of $PrRu_4Sb_{12}$ samples shows that, this compound behaves like regular metallic compounds in the normal state and WF law is valid at very low temperature range.

## 6.1 Electrical resistivity of $PrRu_4Sb_{12}$

The electrical resistivity of $PrRu_4Sb_{12}$ samples were measured between room temperature and 1.5 K. The dimensions of the samples which are labeled A and B were $1250 \times 290 \times 90\mu m$ and $2500 \times 188 \times 380\mu m$ respectively. Sample B had a well–defined cubic shape in contrast to sample A which had a trapezoidal cross section that made the calculation of geometric factor difficult. We used an average value for the thickness of sample A. Fig.6.3 displays the resistivity curves of

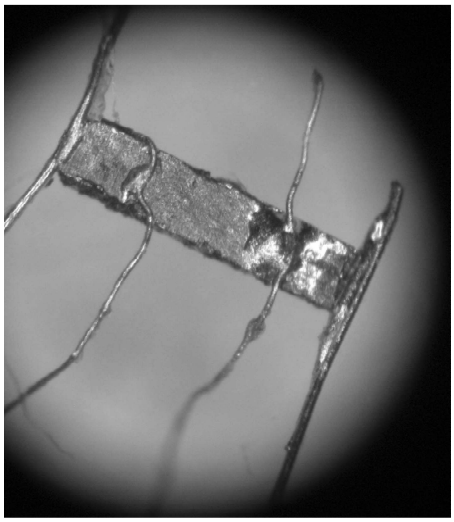

Figure 6.1: Big solder joints in the first sample of $PrRu_4Sb_{12}$ is the biggest error source

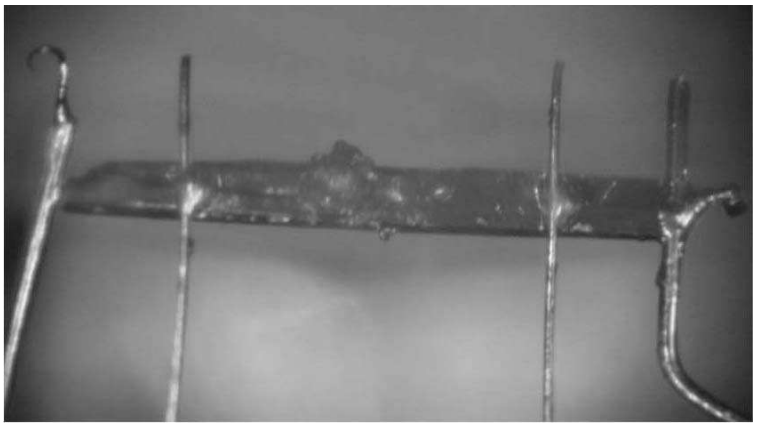

Figure 6.2: Second sample of $PrRu_4Sb_{12}$

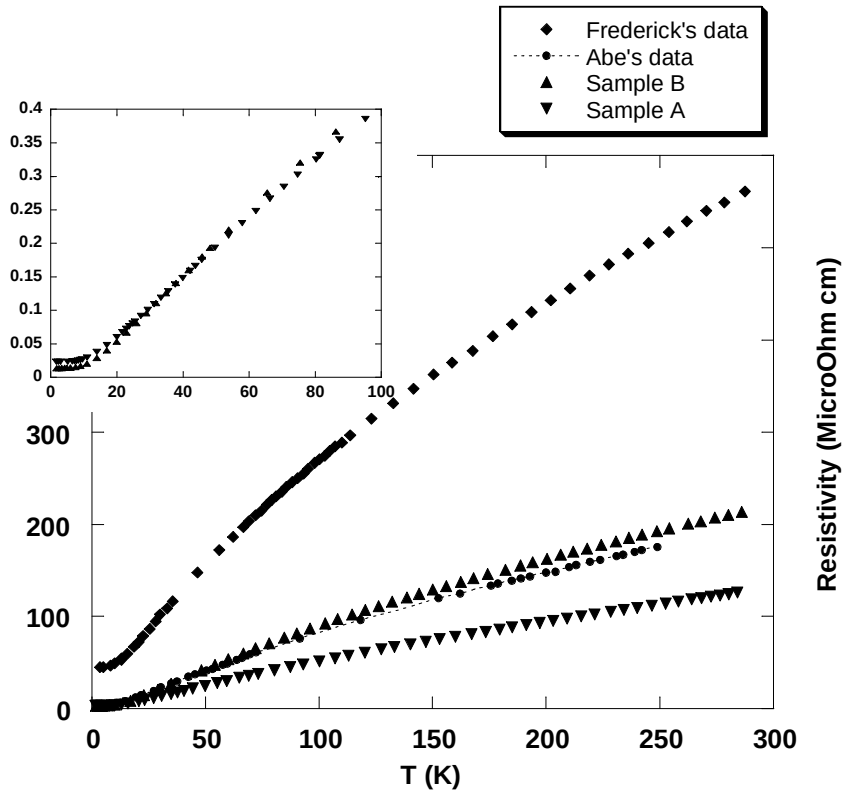


Figure 6.3: Electrical resistivity of our $PrRu_4Sb_{12}$ samples together with Frederick's and Abe's resistivity data. The inset in fig.3 shows the normalized resistivities of sample A and B to room temperature values and since they become quantitatively similar after normalizing, the difference in the actual values before normalizing might be related to the inaccuracy in geometric factors. The geometric factor ($\frac{l}{A}$) of sample A and B were 20768 $m^{-1}$ and 29955 $m^{-1}$ respectively

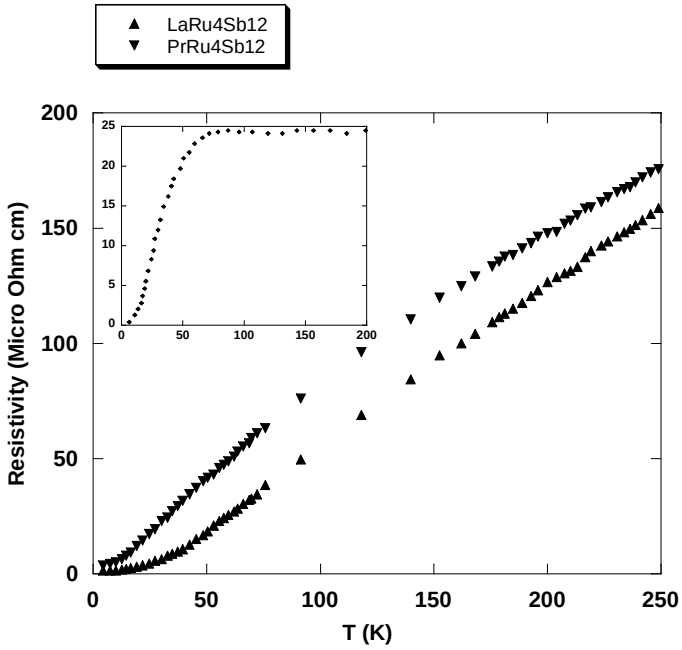


Figure 6.4: Temperature dependence of electrical resistivity of $PrRu_4Sb_{12}$ and $LaRu_4Sb_{12}$, the inset shows the magnetic part of the electrical resistivity estimated by subtracting the phonon contribution from the total resistivity. All data are quoted from [18]

both samples along with two more resistivity curves from [17] and [18]. The $T_c$ was reported 1.08 K at the middle of the superconducting transition in the electrical resistivity measurements [17]. One could see that both samples display the same qualitative behavior versus temperature. As the temperature is reduced, the resistivity decreases which is the typical behavior observed for the metallic compounds. Below 8 K, where a plateau comes up impurities play the dominant role for scattering the electrons. Sample A and B behaves quantitatively very similar to Abe's data. Although they are qualitatively similar to the Frederick's data–set, there is a slight quantitative difference between them. The residual and room temperature resistivities were measured 4.9 $\mu\Omega cm$ and 127 $\mu\Omega cm$ for sample A and 2.9 $\mu\Omega cm$ and 215 $\mu\Omega cm$ for sample B. The residual resistivity ratio are 26 and 74 for sample A and B respectively which are comparable to 25 reported in [17] and 100 reported in [18]. At low temperature range, the main contribution to the electrical resistivity belongs to electron–impurity interactions which is elastic and sample dependent and at high temperatures, the lattice vibrations which is sample independent has the largest effect on scattering the electrons, so the high RRR can be a sign of high purity level of a sample. It has been mentioned in [17] that the residual resistivity ratio of the sample used in their measurements is unusually low and is not completely understood.

The magnetic resistivity of $PrRu_4Sb_{12}$, estimated by subtracting the phonon contribution from total resistivity, increases sharply with increasing temperature and makes a "roll–off" feature at 80 K [18]. This temperature dependence can be related to the increase of the magnetic scattering of the conduction electron by magnetic moment of $Pr^{+3}$ ions which is associated with crystalline electric field (CEF) effects. This feature in magnetic resistivity of $PrRu_4Sb_{12}$ is similar to the "roll-off" feature in the resistivity of $PrOs_4Sb_{12}$ that is discussed in the chapter on electrical resistivity of $PrOs_4Sb_{12}$. The difference is that the effect of the CEF on scattering conduction electrons for $PrOs_4Sb_{12}$ happens at about 10 K and for $PrRu_4Sb_{12}$

about 80 K. This difference might be the result of the difference between the size of Ru and Os atoms. Since the Ru atoms are smaller the hybridization between the conduction and f electrons happens in a smaller scale in comparison with what happens in $PrOs_4Sb_{12}$. Fig.6.4 shows the electrical resistivity of $PrRu_4Sb_{12}$ and $LaRu_4Sb_{12}$ and the CEF contribution which can be taken off by subtracting the lattice contribution from the total resistivity. Above 100 K, since the CEF contribution to the the electrical resistivity saturates, scattering of conduction electrons by the lattice vibrations is expected to make the dominant contribution to resistivity. So one can model the resistivity of $PrRu_4Sb_{12}$ as,

$$\rho(T) = \rho_{imp} + \rho_{CEF} + \rho_{e-g}, \tag{6.1}$$

where $\rho_{imp}$ occurs at very low range and $\rho_{CEF}$ and $\rho_{e-ph}$ in the middle and high temperature range. Comparing to $PrOs_4Sb_{12}$ one can notice the absence of $\rho_{e-e}$ term which is the resistivity due to the electron–electron interaction. In order to have an estimation of the electron–electron scattering one can look at the Kadowaki-woods ratio which is defined as $\frac{A}{\gamma^2}$ [27], where A is defined in $\rho_{e-e} = AT^2$ and $\gamma$ is the coefficient of the electronic specific heat. The Kadowaki-Woods ratio is a universal constant as the physics that gives rise to both of them is the same. Assuming it is almost the same for both $PrRu_4Sb_{12}$ and $PrOs_4Sb_{12}$ one can look at the following fractions,

$$\frac{A(PrOs_4Sb_{12})}{A(PrRu_4Sb_{12})} \sim \frac{\gamma^2(PrRu_4Sb_{12})}{\gamma^2(PrOs_4Sb_{12})}. \tag{6.2}$$

Since $\gamma(PrRu_4Sb_{12}) = 59\ mJ/mol.K^2$ [20], $\gamma(PrOs_4Sb_{12}) = 421\ mJ/mol.K^2$ [21] and $A(PrOs_4Sb_{12}) = 0.009\ \mu\Omega cmK^2$ [28] one can see that $A(PrRu_4Sb_{12}) \sim 1.77E-4\ \mu\Omega cmK^2$ which is not measurable. So the electron–electron interaction is being hidden by scattering of conduction electrons by The CEF and lattice.

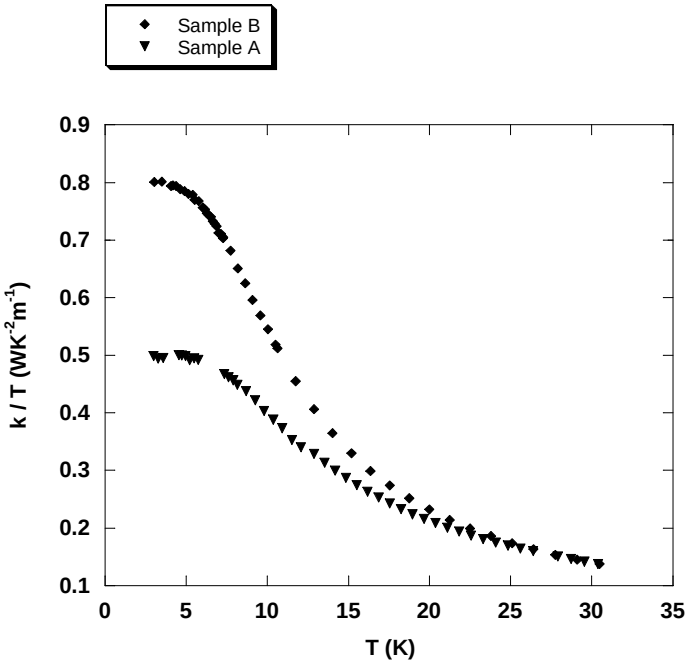


Figure 6.5: Thermal conductivity divided by temperature vs. temperature of both samples

## 6.2 Thermal conductivity measurements of $PrRu_4Sb_{12}$

Fig.6.5 shows the temperature dependence of $\kappa(T)/T$ of both samples up to 30 K. One can recognize features similar to that of silver sample in $\kappa(T)/T$ of $PrRu_4Sb_{12}$. The linear temperature term in thermal conductivity increases by reducing the temperature and ends up to a plateau below 5 K. The existence of the same qualitative features like those that were observed in the thermal conductivity of the silver could lead us to a similar scenario here. As the temperature comes down, scattering of conduction electrons by lattice vibrations decreases and the decrease in electron–phonon interaction which is the most remarkable scattering mechanism against the heat conductivity of electrons, at this temperature range, gives rise to an an increase in electronic thermal conductivity which depends on temperature as $T^{-2}$. As a result the electronic thermal conductivity increases until it reaches a maximum and saturates there. It is scattering by impurity ions which confines the electronic heat transport at very low temperatures. As displayed in fig.6.5, thermal conductivity of both samples shows the same qualitative features versus temperature. Fig.6.6 shows both the charge and heat conductivities of sample B as a function of temperature. It can be seen that the plateau in $\kappa(T)/T$ comes up below 5 K, where the residual resistivity shows up. One can notice that the different limiting low temperature values of $\kappa(T)/T$ are caused by the same differences in the residual resistivity and hence one can see that the WF law is satisfied in the sense that one obtains the Sommerfeld value of the Lorenz number in both cases. Fig.6.7 displays the temperature dependence of Lorenz ratio of both sample A and B. Below 5 K where we have elastic collisions of electrons to impurity ions, thermal conductivity is a linear function of temperature and electrical resistivity is a constant, WF law holds and $\kappa\rho/T = L_0$, where $\kappa = \kappa_e$. As the temperature goes up and thermal vibration of lattice increases, phonons start to take a

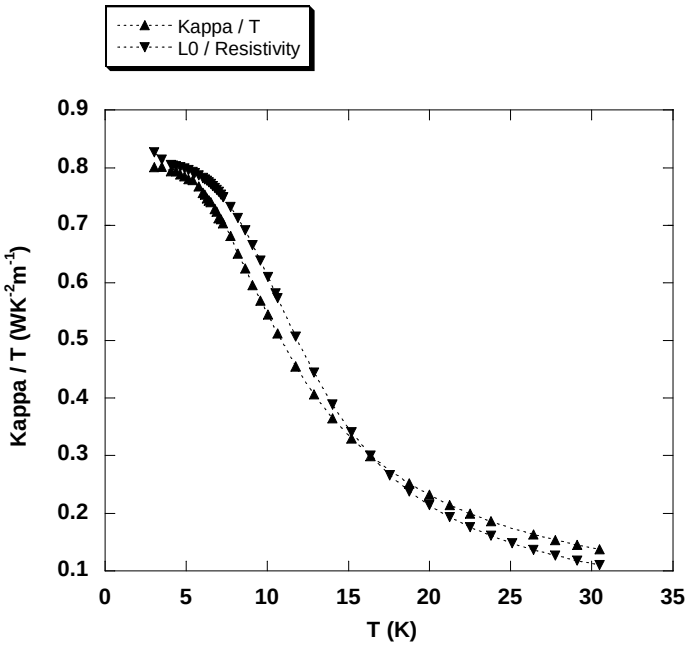


Figure 6.6: $\kappa(T)/T$ and $L_0/Resistivity(T)$ of sample B as a function of temperature

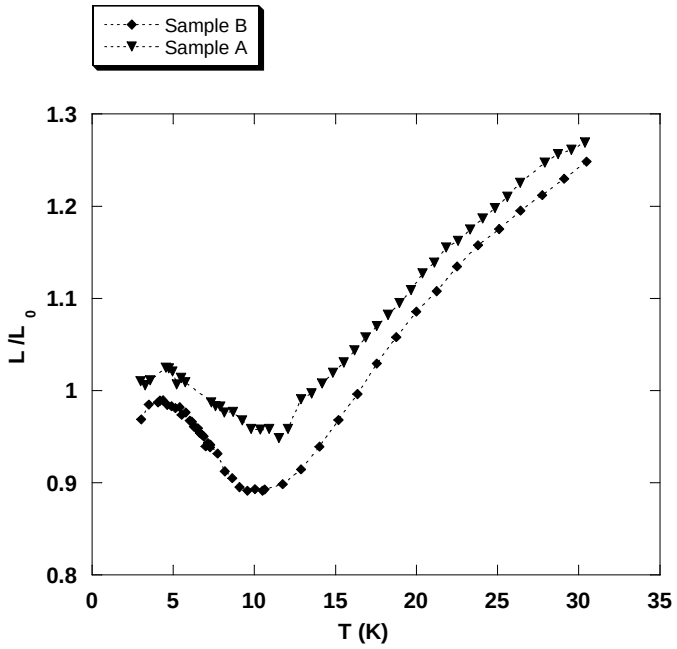


Figure 6.7: Lorenz ratio of $PrRu_4Sb_{12}$ samples as a function of temperature

role in both thermal conductivity and scattering of conduction electrons and the electron–phonon scattering becomes the most dominant scattering mechanism. At this point $\kappa(T) = \kappa_e + \kappa_g$ and $\kappa\rho/T = L(T)$ where L(T) is smaller that $L_0$. As one can notice there is an offset between two curves of fig.6.7 which changes slightly with temperature and takes its maximum when the Lorenz ratio is minimum. It is also know about metallic compounds that the more pure the specimen is, the deeper the minimum of Lorenz ratio will be. One might relate the deeper minimum of sample B to the higher purity level of this sample comparing to sample A.

It is also useful to make a comparison between the temperature dependence of Lorenz ratio of $PrRu_4Sb_{12}$ and $PrOs_4Sb_{12}$. Fig.6.8 displays the the Lorenz ratio of sample B of $PrRu_4Sb_{12}$ and that which was reported for $PrOs_4Sb_{12}$ in [34]. The data of $PrRu_4Sb_{12}$ is taken above the superconducting temperature and below

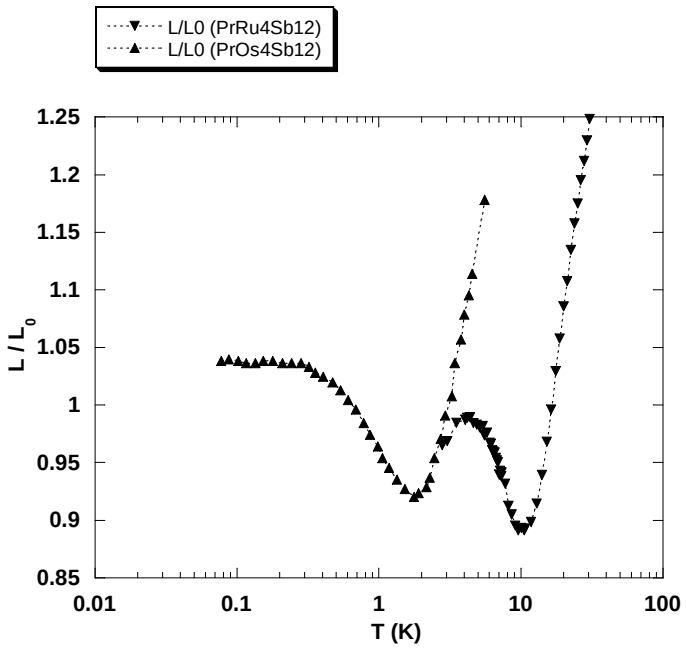


Figure 6.8: The temperature dependence of Lorenz ratio of sample B of $PrRu_4Sb_{12}$ and that reported in [29] for $PrOs_4Sb_{12}$

transition temperature for $PrOs_4Sb_{12}$. One can see the same qualitative features in both of them. One can discuss the temperature dependence of $\frac{L}{L_0}$ in terms of the temperature this minim occurs at.

The plateau in $\frac{L}{L_0}$ shows the predominance of elastic scattering and starts to deviate from 1 as soon as an inelastic mechanism starts scattering electrons. It happens for $PrOs_4Sb_{12}$ at about 0.3 K and for $PrRu_4Sb_{12}$ at about 4 K. This inelastic scattering mechanism can be either phonons or other electrons or $Pr^{+3}$ ions in this case.

−If the minimum is the effect of phonons, it should reflects Debye temperatures which are 232 K and 186 K for $PrRu_4Sb_{12}$ and $PrOs_4Sb_{12}$ respectively.

−The strong electron–electron scattering might be the case in $PrOs_4Sb_{12}$, though if it is true, then it should happen at the same temperature range that the electronic specific heat takes its high value. It can not be true in case of $PrRu_4Sb_{12}$ as there is no evidence for strong electron–electron interaction at this temperature range for $PrRu_4Sb_{12}$.

−The scattering of electrons by $Pr^{+3}$ ions happens in both systems and the "roll–off" temperature differs by a factor of $\sim 10$ between them. However whether the scattering starts at the appropriate temperatures (0.3 K for $PrOs_4Sb_{12}$ and 4 K for $PrRu_4Sb_{12}$) is difficult to determine, since the resistivity curves show where the "roll–off" start but not where they end. This needs further calculations.

In conclusion, thermal conductivity of $PrRu_4Sb_{12}$ shows no anomalies in the normal state up to 30 K. Although the resistivity plots reported on different samples with different purity levels show the same qualitative features, but we still do not have any explanation in the difference between room temperature resistivities of samples of this measurements and those reported elsewhere.

# Chapter 7

# Conclusion

In this study we have presented and compared the heat and charge conductions of single crystals of $PrRu_4Sb_{12}$ and $PrOs_4Sb_{12}$. The Wiedemann-Franz law was investigated for both of these compounds in 1.1–35 K range.

−The measurement of electrical resistivity of $PrRu_4Sb_{12}$ above $T_c = 1.1K$ shows that this compounds behaves similarly to regular metallic compounds where the resistivity decreases with reducing the temperature. The resistivity was shown to be qualitatively like previous data in the literature and part of the quantitative difference could be due to the differences in purity levels.

−The thermal conductivity of $PrRu_4Sb_{12}$ also behaves like regular metallic compounds (like silver) and decreases with decreasing the temperature. Impurities were shown to be the dominant scattering mechanism against electrons at low temperatures.

−The resistivity data on $PrOs_4Sb_{12}$ is quantitatively and qualitatively in agreement with previous published data and decreases with decreasing the temperature. The Fermi liquid behavior was observed in 8–45 K range. The effect of crystalline electric field on resistivity was discussed in terms of the "roll-off" feature which was

observed at about 8 K.

−The measurements on thermal conductivity of $PrOs_4Sb_{12}$ were done in 1.1–35 K and the feature in thermal conductivity were discussed in terms of contributions of both electrons and phonons. The highest temperature peak which occurs around 13 K fits very well with a change in the phononic contribution to the heat transport. The peak at $T_c$ can be due to a decrease in number of normal electrons and the peak at 0.8 K could also have an electronic origin in terms of an increase in the quasiparticle mean free path due to a decrease in electron–electron scattering. Since some specific heat and angle resolved magneto-thermal conductivity measurement measurements shows a double jump below $T_c = 1.81K$, the lowest temperature peak might also be related to entering to a new superconducting phase. To identify the origin of this the extremums below $T_c$ one needs to do more measurements as the reports in the literature indicates sample dependence.

# Bibliography


[1] B. C. Sales et. al., Science, 272, 1325-1327, (1996)

[2] Ashkroft and Mermin, Solid state physics, (1979)

[3] R. Berman, Thermal conduction in solids, Clarendon Press, Oxford, (1976)

[4] J. M. Ziman, Principles of the theory of solids, Cambridge University Press, (1999)

[5] P. G. Klemens, Solid state physics, (1956)

[6] H. M. Rosenberg, Low temperature solid state physics, Oxford at the clarendon press, (1965)

[7] J. Bardeen, L. N. Cooper and J. R. Schriffer, Phys. Rev., 108, (1975)

[8] M. Tinkham, Introduction to superconductivity, Dover Publication, (2004)

[9] J. Bardeen, G. Rickayzen, L. Tewordt, Phys. Rev., 113, 4, (1959)

[10] M. J. Graf et. al., PRB 53, 22, 15147 (1996)

[11] P. A. Lee, Phys. Rev. Lett. 71, 1887 (1993)

[12] L. Tewordt and T. Wolkhausen, Solid State Communications, 70, 839, (1989)

[13] Frank Pobell, Matter and Methods at Low Temperature. Springer Publication, (1996)

[14] D. L. Rule et. al., Cryogenics 36, 283 (1996)

[15] G.K. White. Experimental Techniques in Low Temperature physics. clarendon Press, Oxford, (1968)

[16] M. Davenport, Calibrating the Lakeshore 331 temperature controller, Co–op report, (2004)

[17] N. A. frederick et. al., PRB 69, 024523 (2004)

[18] Abe et. al., J. Phys:condens. matter 14 11757 (2002)

[19] E. D. Bauer et al, J. Phys.:Condens. Matter 13 5183 (2001)

[20] Takeda et. al., J. Phys. Soc. Japan, 69, 3, 868 (1999)

[21] N. A. frederick et. al., PRB 71, 064508 (2005)

[22] Elbert E. M. Chia et. al.,arXiv:cond-mat/0402610 v1 (2006)

[23] Izawa et. al., PRL 90, 117001 (2003)

[24] G. Seyfarth et al, PRL 95 107004 (2005)

[25] M. A. Measson et. al., Physica B, 378-380, 56-57 (2006)

[26] M. B. Maple et al,J. Phys.:Condens. Matter 15 2071 (2003)

[27] Yuji Aoki et. al., J. Phys. Soc. Japan, 74, 1, 209 (2005)

[28] N. A. Frederick and M. B. Maple, J. Phys.:Condens. Matter 15 4789 (2003)

[29] Seyfarth et. al., arXiv:cond–mat/067561 (2006)

[30] K. W. H. Stevens, Proc. Phys. Soc. LXV, 3-A (1951)

[31] Aronson et. al, J. Appl. Phys. 69, 8 (1991)

[32] K. R. Lea et. al., J. Phys. Chem. Solids 23, 1381 (1962)

[33] Fulde P and Loewenhaupt M 1986 Adv. Phys. 34 589 (1986)

[34] G. Seyfarth et al, PRL 95 107004 (2005)

[35] Benoit Lussier et. al., PRL 73, 3294 (1994)

[36] D. Parker et. al., Cond-mat/0604493 (2006)

[37] Vollmer et. al., PRl 90, 057001 (2003)

[38] R.C.Yu et. al., PRL 69, 1431 (1992)

[39] P.J. Hirschfeld et. al., PRL 77 3909 (1996)

[40] R. W. Hill et. al., unpublished

[41] M. Suzuki et. al.,PRL 88, 227004 (2002)

[42] M. Tanatar et. al., PRL 95, 067002 (2005)